Proteasome inhibition can induce an autophagy-dependent apical activation of caspase-8

Markus Rehm, Maike Anne Laussmann, Judith Anna Rauen, Heiko Dussmann, Maximimilian Wurstle, Egle Passante, Marc Devocelle, Jochen H.M. Prehn, Maria Eugenia Delgado

Proteasome inhibition can induce an autophagy-dependent apical activation of caspase-8

Running Title: Caspase-8 activation upon proteasome inhibition

Maike A. Laussmann[1], Egle Passante[1], Heiko Düssmann[1], Judith A. Rauen[1], Maximilian L. Würstle[1], Maria Eugenia Delgado[1], Marc Devocelle[2], Jochen H. M. Prehn[1], Markus Rehm[1,*]

[1]Department of Physiology & Medical Physics, Royal College of Surgeons in Ireland, Dublin 2, Ireland; [2]Centre for Synthesis and Chemical Biology, Department of Pharmaceutical & Medicinal Chemistry, Royal College of Surgeons in Ireland, Dublin 2, Ireland

* To whom correspondence should be addressed.

Dr. Markus Rehm

Department of Physiology and Medical Physics

Royal College of Surgeons in Ireland

RCSI York House, York Street

Dublin 2, Ireland

Phone: +353-1-402-8563

Fax: +353-1-402-2447

E-mail: mrehm@rcsi.ie

Key Words: Apoptosis, Caspase-8, Bortezomib, Proteasome, Autophagy, Bcl-2, XIAP, Atg5, Förster resonance energy transfer (FRET).

Abstract

Anti-apoptotic Bcl-2 family proteins are often highly expressed in chemotherapy-resistant cancers and impair mitochondrial outer membrane permeabilisation (MOMP), a key requirement for caspase activation via the intrinsic apoptosis pathway. Interestingly, while Bcl-2 overexpression in HeLa cervical cancer cells abrogated caspase processing in response to intrinsic apoptosis induction by staurosporine, tunicamycin or etoposide, residual caspase processing was observed following proteasome inhibition by bortezomib, epoxomicin or MG-132. Similar responses were found in Bcl-2 overexpressing H460 NSCLC cells and Bax/Bak-deficient mouse embyronic fibroblasts. Mild caspase processing resulted in low DEVDase activities, which were MOMP independent and persisted for long periods without evoking immediate cell death. Surprisingly, depletion of caspase-3 and experiments in caspase-7-depleted MCF-7-Bcl-2 cells indicated that the DEVDase activity did not originate from effector caspases. Instead, FADD-dependent caspase-8 activation was the major contributor to the slow, incomplete substrate cleavage. Casapse-8 activation was independent of death ligands but required the induction of autophagy and the presence of Atg5. Depletion of XIAP or addition of XIAP-antagonizing peptides resulted in a switch towards efficient apoptosis execution, suggesting that the requirement for MOMP was bypassed by activating the caspase-8/caspase-3 axis. Combination treatments of proteasome inhibitors and XIAP antagonists therefore represent a promising strategy to eliminate highly resistant cancer cells which overexpress anti-apoptotic Bcl-2 family members.

Introduction

Proteasomal protein degradation is essential for eliminating excess proteins and, by counteracting protein production, establishes steady-state protein levels during cellular homeostasis. The selective and often well timed degradation of regulatory proteins by the proteasome machinery orchestrates and modulates a multitude of biological processes such as gene transcription, oxidative metabolism, cell cycle progression, and cell differentiation (1-2). Prolonged proteasome inhibition induces stress responses which initiate apoptosis signalling via the intrinsic apoptosis pathway. This is exploited clinically in the treatment of multiple myeloma with the proteasome inhibitor bortezomib. Impairment of proteasome-mediated protein degradation results in the accumulation and/or transcriptional induction of BH3-only proteins such as Puma, Bim, Noxa, or Bik in various malignant human neoplasms, including multiple myeloma, neuroblastoma, lymphoma or leukaemia (3-6). BH3-only proteins antagonise anti-apoptotic Bcl-2 family members such as Bcl-2, Bcl-xL or Mcl-1 and/or can activate the pro-apoptotic members Bax and Bak (7). Activated Bax and Bak form pores in the outer mitochondrial membrane, resulting in cytochrome-c, Smac/Diablo and HtrA2/Omi release from the intermembrane space into the cytosol. This results in caspase-9 activation, inhibition of inhibitor-of-apoptosis (IAP) proteins, and subsequent apoptosis execution by effector caspases (7). Proteasome inhibitors were shown to evoke synergistic cell killing in combinations with other drugs that induce the intrinsic apoptosis pathway, such as cisplatin, doxorubicin, paclitaxel, or histone deacetylase inhibitiors (8-11), as well as with death receptor ligands activating the extrinsic pathway, such as TRAIL and Fas-L (12-15). While the molecular mechanisms bringing about the synergistic responses in these

scenarios are still under investigation, evidence has accumulated that synergies may emanate from complementary sets of BH3-only proteins being induced or may result from more efficient formation of the death inducing signalling complex (DISC) in response to the addition of death ligands.

Proteasome inhibition however may also promote more efficient apoptotic cell death through the stabilisation of proapoptotic proteins implicated in apoptosis execution. Following mitochondrial permeabilisation, cytosolic Smac/Diablo and maybe also active caspases-9, -3, and -7 are subject to rapid IAP-mediated proteasomal degradation (16-17). Likewise, cytosolic cytochrome-c is swiftly degraded but can be stabilised by proteasome inhibition (18). Here we investigated the consequences of proteasome inhibition on caspase activation and activity in human cancer cells. We demonstrate that in Bcl-2 overexpressing cancer cells refractory to mitochondrial permeabilisation, prolonged proteasome inhibition induced a mild, death-ligand independent but autophagy dependent caspase-8 activation, which, upon antagonising XIAP, can be exploited to eliminate Bcl-2-overexpressing cells via the caspase-8/-3 axis.

Results

Proteasome inhibition promotes residual processing of procaspase-3 in human cancer cells expressing high levels of Bcl-2.

We investigated apoptosis signalling in response to proteasome inhibition by analysing the conversion of the caspase-3 zymogen into active subunits. Processing of procaspase-3 results in the generation of the small p12 and large p20 active subunits, with the latter being further processed first to the p19 and then to the p17 fragment by rapid and slow autocatalytic steps, respectively (19). Initially, we induced the intrinsic mitochondrial pathway of apoptosis in parental HeLa cervical cancer cells by broad spectrum kinase inhibitor staurosporine (STS), N-glycosylsation inhibitor tunicamycin, topoisomerase II inhibitor etoposide, or proteasome inhibitor bortezomib. All drugs resulted in apoptosis execution in parental HeLa cells, as noticed by processing of procaspase-3 into the active caspase-3 p19/p17 subunits (Fig.1A). Particularly strong responses were observed upon STS and bortezomib treatment (Fig.1A). We then employed human cancer cells overexpressing Bcl-2 (Supplemental Fig.1) as model systems that are highly resistant to drugs inducing the intrinsic apoptosis pathway. Overexpression of Bcl-2 fully abrogated procaspase-3 processing in response to all drugs except bortezomib. Bortezomib still evoked residual and incomplete procaspase-3 processing in HeLa-Bcl-2 cells (Fig.1A, arrows). Caspase-3 processing was attenuated at the p20/p19 subunits (Fig.1A, arrows), indicating that the final and slow autocatalytic step towards the fully mature p17 subunit was suppressed (19). Similar results were obtained when investigating other durations of bortezomib exposure or when employing other proteasome inhibitors such as epoxomicin or MG-132 (Fig.1B-D). Residual procaspase-3

processing was also observed in human H460 non-small-cell lung cancer cells overexpressing Bcl-2 when exposed to bortezomib (Fig.1E), but not when incubated with STS (not shown), and in Bax/Bak double deficient mouse embryonic fibroblasts (MEFs) (Fig.1F). Bcl-2 overexpression or Bax/Bak deficiency reduced bortezomib-induced cell death, and a further reduction was observed when adding caspase inhibitor zVAD-fmk (Fig.1G-I). Taken together, these results indicate that proteasome inhibition can provoke a late and residual accumulation of incompletely processed subunits of effector caspase-3 as well as limited amounts of cell death in cells which otherwise seem refractory to intrinsic apoptosis signalling. In the following we therefore further characterised the mode of caspase activation through proteasome inhibition in MOMP-impaired cells. Due to its high apoptotic potency in HeLa cells (Fig.1A), we used STS in control groups as a model for classical MOMP-dependent apoptosis, but avoided treatment durations that result in secondary cell death arising from prolonged broad range kinase inhibition (20) (Supplemental Fig.2).

Proteasome inhibition induces low levels of DEVDase activity in Bcl-2 over-expressing cells.

To investigate whether the detected caspase processing resulted in any noticeable caspase activity, we next measured DEVD substrate cleavage by flow cytometric measurements of Förster resonance energy transfer (FRET) disruption (21). In the recombinantly expressed FRET substrate, a caspase cleavage site (DEVD) links donor and acceptor fluorophores [cyan and yellow fluorescent protein (CFP, YFP)], and loss of FRET evokes an increase in CFP fluorescence (Fig.2A). The DEVD sequence represents the optimal cleavage motif for effector caspases-3 and -7, but it can also be cleaved by initiator caspase-8 (22). Of note, since the FRET probe is a soluble

cytosolic protein, the FRET analysis is restricted to cells which have not yet undergone plasma membrane permeabilisation. As expected, in parental HeLa cells bortezomib and STS resulted in FRET probe cleavage in nearly all cells (Fig.2B). In cells over-expressing Bcl-2, FRET probe cleavage could be detected in a smaller but still substantial fraction of the bortezomib-treated cell population (Fig.2C). Addition of caspase inhibitor zVAD-fmk potently inhibited probe cleavage and confirmed the caspase specificity of the readout. Similar responses were also detected in Bax/Bak deficient MEFs (Fig.2D).

Closer inspection of CFP vs. FRET scatter plots obtained from bortezomib-treated samples indicated further differences in substrate cleavage between parental and Bcl-2 over-expressing HeLa cells (Fig.2E,F). In parental cells, populations with intact or cleaved FRET probe could be clearly separated (Fig.2E), indicative of a caspase-3 dependent rapid all-or-none probe cleavage as has been described in response to other apoptotic stimuli previously (21). In contrast, scatter plots of HeLa-Bcl-2 cells highlighted that a significant number of cells showed submaximal probe cleavage at the time of sample reading, i.e. they were positioned in-between populations with intact and cleaved probe (Fig.2F). Conversion of the scatter data into a ratiometric CFP/FRET display likewise indicated that parental cells either displayed with intact or cleaved probe, whereas in HeLa-Bcl-2 cells the two populations could no longer be separated (Fig.2G,H). These results therefore suggest that proteasome inhibition is potent to induce low amounts of DEVDase activity in cells that otherwise do not respond to intrinsic apoptosis initiation.

Time-lapse analysis of DEVDase activation and activity induced by proteasome inhibition.

Immunoblotting and flow cytometry measurements are limited in temporal resolution and do not allow to investigate sequential events in individual cells over time. We therefore employed FRET-based single-cell time-lapse microscopy to determine the kinetics and timings of DEVDase activation with high temporal accuracy. HeLa cells were monitored for up to 72 h following proteasome inhibition. An initial analysis indicated that most cells responded with DEVDase activation during this time, independent of whether Bcl-2 was overexpressed or not (Fig.3A). However, DEVDase activity in HeLa cells overexpressing Bcl-2 started later than in parental HeLa cells (Fig.3B). On average, Bcl-2 overexpression delayed bortezomib-induced DEVDase activation by 14 h +/- 3.2 h (mean +/- s.e.m.). Once initiated, DEVD FRET probe cleavage proceeded rapidly in parental HeLa cells (14.7 min +/- 1.0 min; mean +/- s.e.m.), indicating a swift and efficient activation of effector caspases (Fig.3C). Similar cleavage durations were measured in response to activation of the intrinsic apoptosis pathway by STS (11.5 min +/- 0.7 min; mean +/- s.e.m.; n = 21 cells analysed from 3 experiments), corresponding to previously published data (23). In contrast, probe cleavage in HeLa-Bcl-2 cells appeared to proceed significantly slower (81.3 min +/- 13.4 min; mean +/- s.e.m.) (Fig.3C). We noticed that in many of these cells the cleavage process might not have reached completion before termination of image acquisition since many cells detached and left the focal plane late during substrate cleavage. We therefore additionally determined the slopes of the FRET disruption traces to measure DEVDase activity. This analysis indeed showed that DEVDase activity was significantly reduced in HeLa-Bcl-2 cells (Fig.3D). Additional evidence that substrate cleavage was submaximal in HeLa-Bcl-2 cells was obtained when analysing floating cells by Western blotting. Western blotting indicated that

floating HeLa-Bcl-2 cells presented with only partially cleaved DEVD probe, while in parental HeLa cells the FRET substrate was fully cleaved (Supplemental Fig.3).

We also loaded cells with tetramethylrhodamine-methyl-ester (TMRM), a non-toxic, cationic dye, to monitor changes in mitochondrial membrane potentials. As the mitochondrial membrane potential rapidly drops upon cyt-c release at standard experimental conditions (24), TMRM here was used to indirectly measure mitochondrial outer membrane permeabilisation (MOMP). As expected, in HeLa cells treated with STS, DEVDase activity was exclusively detected subsequent to the onset of mitochondrial depolarisation (3.2 min +/- 0.4 min lag time; mean +/- s.e.m.), corresponding to earlier reports (23). Similarly, proteasome inhibition in the majority of parental HeLa cells resulted in DEVDase activity subsequent to onset of mitochondrial depolarisation (Fig.3E) (mean lag time 3.6 min +/- 0.6 min s.e.m.). Only a small subpopulation of parental HeLa cells (5 out of 32 cells) displayed DEVDase activity 5.6 min +/- 3.6 min (mean +/- s.e.m.) before a decrease in the TMRM signal. In HeLa-Bcl-2 cells instead DEVDase activation seemed to occur nearly exclusively upstream of changes in mitochondrial TMRM signals (Fig.3F) (20 out of 21 cells = 95%), and DEVDase activity persisted until cells left the focal plane or the image acquisition was terminated. To further validate this finding we also observed MOMP more directly using cells transiently transfected to express a red fluorescent mitochondrial intermembrane space protein (IMS-RP) in parallel to the DEVD FRET probe. In parental HeLa cells IMS-RP release started shortly before DEVDases were activated (Fig.3G). In contrast, DEVDase activation in HeLa-Bcl-2 cells was detected nearly exclusively independent of IMS-RP release (14 out of 15 cells = 93%) (Fig.3H). To validate whether also cell-endogenous caspase substrates were cleaved, we investigated the cleavage of α-spectrin, a substrate preferred by

effector caspase-3. In parental cells the 120 kDa cleavage fragment accumulated strongly, whereas in Bcl-2 overexpressing cells only a mild increase at late times could be detected (Fig.3I). Taken together these data indicated that proteasome inhibition resulted in a mild, submaximal activation of DEVDases independent of MOMP.

MOMP-independent DEVDase activity in response to proteasome inhibition does not arise from caspase-3 or -7.

We next set out to identify which caspases contributed to DEVDase activity in response to proteasome inhibition by employing siRNA-mediated depletion of protein expression. All siRNA sequences used were previously published and were shown to be specific for their respective targets (see methods and Supplemental Material 1). In initial optimisation experiments multiple concentrations of siRNAs were co-transfected together with pCFP-DEVD-YFP and cells were analysed by immunoblotting for conditions that resulted in maximal protein depletion. For all subsequent experiments the addition of bortezomib was timed so that the target proteins were strongly depleted before residual caspase processing set in (see methods and Supplemental Fig.8).

As caspase-3 is the most efficient DEVDase known, we first depleted HeLa-Bcl-2 cells of procaspase-3 expression (Fig.4A, Supplemental Fig.8A). Interestingly, depletion of caspase-3 did not reduce DEVDase activity arising from bortezomib exposure (Fig.4B). Likewise, time lapse imaging of HeLa-Bcl-2 cells indicated that the frequency of DEVDase activation was not notably affected by caspase-3 depletion (see Fig.5F). In control experiments, the depletion of procaspase-3 achieved by our siRNA approach however was sufficient to impair TRAIL/CHX-induced apoptosis in

parental HeLa cells (Supplemental Fig.4). We next also employed caspase-3 deficient MCF-7 cells overexpressing Bcl-2 to investigate DEVD FRET substrate cleavage in response to bortezomib. Consistent with results shown for HeLa and H460 cells, control experiments showed that MCF-7-Bcl-2 cells but not parental MCF-7 cells were refractory to apoptosis and DEVD FRET probe cleavage induced by STS (Supplemental Fig.5). We then went on to deplete MCF-7-Bcl-2 cells of procaspase-7 (Fig. 4C, Supplemental Fig.8B) to eliminate all DEVD-preferring effector caspases. Interestingly, independent of presence or absence of caspase-7, proteasome inhibition resulted in cells localising across a continuous spectrum from intact to cleaved DEVD substrate (Fig.4D). Taken together, these data therefore indicate that the cleavage of the FRET probe apparently does not depend on a significant activation of caspases-3 or -7, the major DEVDases amongst the caspases.

MOMP-independent DEVDase activity in response to proteasome inhibition arises from FADD-dependent caspase-8 activation.

We next tested whether initiator caspase-8 would be involved in generating the caspase activity we observed, since caspase-8 is known to possess substantial DEVDase activity (22). Procaspase-8 was processed into p43/41 and p18 fragments in parental HeLa cells in response to bortezomib (Fig.5A). Procaspase-8 processing correlated with the times of caspase-3 activation (Fig.1B), as would be expected from feed-back processing following caspase-3 activation. In HeLa-Bcl-2 cells only low amounts of cleaved caspase-8 were detected (Fig.5B). The cleavage of Bid, a physiological caspase-8 substrate that can also be truncated by caspase-3, correlated with procaspase-8 processing in both scenarios (Fig.5C). Following experimental optimization, procaspase-8 expression could be successfully suppressed by siRNA

transfection (Fig.5D, Supplemental Fig.8C), and procaspase-8 depletion reduced DEVDase activity in response to proteasome inhibition (Fig.5E), suggesting that caspase-8 is involved in probe cleavage. Likewise, time lapse imaging indicated that procaspase-8 depletion, but not procaspase-3 depletion, massively reduced the amount of cells displaying DEVDase activity (Fig.5F). Furthermore, procaspase-3 processing into p20/p19 subunits was reduced upon procaspase-8 silencing (Fig.5G), as was the overall cell death observed in response to proteasome inhibition (Fig.5H). Even though multiple caspases can cleave DEVD sequences, these data therefore indicate that in response to proteasome inhibition caspase-8 serves as the apical caspase in MOMP-impaired cells.

Activation of caspase-8 requires the dimerisation and autocatalytic processing of procaspase-8 (25), and Fas-associated death domain (FADD) serves as an essential recruitment protein for procaspase-8 dimerisation. We therefore next tested whether caspase-8 activation in response to proteasome inhibition depends on FADD. We achieved a highly efficient siRNA-mediated depletion of FADD in HeLa-Bcl-2 cells (Fig.5I, Supplemental Fig.8D), which resulted in significantly reduced DEVDase activity in response to proteasome inhibition (Fig.5J). In control experiments, depletion of caspase-8 and FADD was sufficient to impair death receptor mediated apoptosis in parental HeLa cells (Supplemental Fig.4), showing that the targeting sequences also confer protection in a canonical apoptosis signalling model. Taken together, these results indicated that the MOMP-independent mild DEVDase activity detected in response to proteasome inhibition arose from FADD-dependent caspase-8 activation.

Apical caspase-8 activation in response to proteasome inhibition is independent of death receptor ligands.

Since FADD was required for caspase-8 activation in response to proteasome inhibition, we next investigated whether canonical death receptor pathways are required to establish apical caspase-8 activity. Proteasome inhibition may induce the secretion of death receptor ligands such as TRAIL, TNF-α or FasL, which may in turn activate caspase-8 by autocrine death receptor activation. To test the involvement of death ligands, we employed neutralising antibodies targeting the death receptors. Pretreatment of parental HeLa cells with neutralizing antibodies was sufficient to fully block caspase-3 processing following TRAIL, TNF-α or FasL exposure (Fig.6A). Pretreatment of HeLa-Bcl-2 cells with the receptor neutralising antibodies alone or in combination, however, did not affect bortezomib-induced residual procaspase-3 processing (Fig.6B,C). These data therefore indicate independence of autocrine death ligand signalling.

Proteasome inhibition induces autophagy, which contributes to caspase-8 processing and cell death.

It has been suggested that autophagy can increase as a compensatory means of protein degradation when the proteasomal pathway is blocked (26). Furthermore, in proliferating T-cells caspase-8, in complex with FADD and receptor-interacting serine/threonine-protein kinase 1 (RIPK1), was found activated on autophagosomal membranes (27). We therefore investigated whether a link between autophagic signalling, caspase-8 processing and cell death could be observed in response to proteasome inhibition.

We found that autophagic flux increased in HeLa Bcl-2 cells following bortezomib exposure, as evidenced by an increase in total levels of autophagy marker protein LC3 and the accumulation of lipidated LC3-II when inhibiting lysosomal proteases using E64 D and pepstatin A (Fig.7A). Accordingly, the amounts of p62, an autophagy adaptor protein and indicator of protein aggregation that is known to accumulate upon proteasome inhibition (28), increased following bortezomib treatment (Fig.7A,B). A further increase, indicative of elevated autophagic flux, was found upon E64 D/pepstatin A addition (Fig.7A). We also observed that the levels of FADD increased strongly, whereas increases in RIPK1 were modest and transient (Fig.7B). RIPK1 is a physiological substrate of caspase-8, and the late loss of RIPK1 could be prevented by the addition of caspase inhibitor zVAD-fmk (not shown). Autophagy induction was also detected in cells expressing a mCherry-GFP-LC3 fusion protein, with the number of GFP-positive punctae, representing autophagosomes, increasing strongly in response to bortezomib (Fig.7C). The GFP fluorescence is quenched upon fusion of autophagosomes with lysosomes, whereas mCherry fluorescence persists (29). The number and intensities of mCherry punctae were visibly higher than the GFP signals (Fig.7C), indicating an increase in autolysosomes and overall autophagic flux.

Increased autophagosome formation was linked to caspase-8 activation, since 3-methyl adenine (3-MA), an inhibitor of the initiation and maturation of autophagosomes, but not necrostatin, a specific inhibitor of RIPK1, strongly reduced procaspase-8 processing (Fig.7D). LC3-I to LC3-II conversion was noticeably impaired, indicating strong inhibition of autophagy at 3-MA/bortezomib co-treatment conditions (Fig.7D). These results therefore show that caspase-8 processing in response to proteasome inhibition strongly depends on autophagy induction. When investigating whether autophagy inhibition by 3-MA also reduced the overall amount

of cell death following bortezomib addition, we observed a mild but nevertheless significant protection (Fig.7E). RIPK1 inhibition in contrast did not reduce cell death (Fig.7E), suggesting that death modalities such as necroptosis or excessive, lethal autophagy arising from increased RIPK1 activities (30-31) did not contribute to cell death here. The reduction in cell death might appear rather modest, however, since prolonged 3-MA exposure on its own was highly potent in inducing apoptosis in parental HeLa cells (Supplemental Fig.6A), and since cell death of HeLa Bcl-2 cells upon bortezomib/3-MA co-treatments was z-VAD-fmk sensitive (Supplemental Fig.6B), it is likely that an alternative form of caspase-dependent cell death, which we do not further characterise here, is synergistically promoted at these conditions.

Given the above results, we next also aimed to block autophagy more specifically by targeted depletion of Atg5. Atg5 is required for autophagosome formation and is found conjugated to Atg12 via an isopeptide bond, and it was suggested that caspase-8 activation during T-cell proliferation requires the FADD-dependent docking to Atg5-Atg12 conjugates on autophagosomal membranes (27). When we depleted HeLa Bcl-2 cells of Atg5 expression, we indeed observed that caspase-8 processing was blocked in response to bortezomib (Fig.7F), and furthermore that cell death was significantly reduced (Fig.7G). Taken together, our data therefore demonstrate that the processing of caspase-8 is strongly impaired when inhibiting autophagy pharmacologically or by Atg5 depletion, indicating that autophagosome formation is one of the main contributors to caspase-8 activation in response to proteasome inhibition.

XIAP depletion and Smac-derived peptides enhance proteasome inhibitor-induced DEVDase activation and apoptosis in Bcl-2 overexpressing cells.

Most cells require the mitochondrial apoptosis pathway to efficiently execute apoptosis. In MOMP-impaired cells, XIAP efficiently prevents caspase-8 mediated processing of procaspase-3 to directly translate into cell death, as was shown in response to death receptor stimulation (32). We therefore hypothesized that DEVDase activity evoked by proteasome inhibition could be enhanced by XIAP depletion or by a XIAP-antagonising Smac peptide. XIAP depletion by siRNA transfection (Fig.8A, Supplemental Fig.8E) indeed significantly enhanced DEVD FRET probe cleavage and increased cell death in response to proteasome inhibition (Fig.8B,C). To circumvent the requirement for transfection procedures, we next synthesized a XIAP antagonising peptide (AVPIA) fused to an HIV-derived import sequence (33) with the intention to sensitize MOMP-impaired cells to proteasome inhibitor induced cell death. Flow cytometric measurements in HeLa-Bcl-2 and H460-Bcl-2 cells indicated that the AVPIA peptide alone did not evoke noticeable cell death (Fig.8D,E), nor did it enhance STS induced cell death at control conditions (Supplemental Fig.7). Co-treatment with AVPIA peptide instead markedly enhanced cell death in response to proteasome inhibition (Fig.8D,E). These results therefore indicate that antagonising XIAP is a promising approach to enhance apoptosis execution in response to proteasome inhibition in highly resistant human cancer cells that overexpress Bcl-2.

Discussion

We identified that proteasome inhibition promotes the FADD-dependent activation of caspase-8 in human cancer cells in which the mitochondrial apoptosis pathway is blocked, and that autophagy induction is an important contributor to caspase-8 activation. Caspase-8 activity is low and persists for long times without leading to immediate apoptosis execution. Cellular commitment to apoptosis can however be promoted by parallel XIAP depletion or by exposure to XIAP antagonising peptides. This treatment strategy therefore allows to circumvent the Bcl-2 mediated inhibition of apoptosis and may provide a promising alternative to restore apoptosis susceptibility in highly resistant human cancer cells which cannot execute apoptosis via the mitochondrial pathway.

Impaired protein degradation by proteasome inhibition affects the relative abundance of hundreds of cellular proteins and is believed to induce apoptosis mainly through the intrinsic mitochondrial pathway by the accumulation of BH3-only proteins (3-6). Our analyses showed that in cells in which the mitochondrial apoptosis pathway is impaired, caspase-8 can be activated in response to proteasome inhibition and that this was the predominant response in the majority of cells investigated. While previous studies already suggested a role for caspase-8 in apoptosis following proteasome inhibition (34-35), time lapse and single cell analyses here unequivocally showed that caspase-8 can act as the apical initiator caspase in this treatment paradigm rather than being activated subsequent to caspase-3, which has largely overlapping substrate specificities (22).

Efficient canonical activation of caspase-8 requires the dimerisation of procaspase-8 and autocatalytic processing at multiprotein recruitment platforms, such as the death inducing signalling complex during extrinsically induced apoptosis (25, 36). We here could show that autophagy induction contributes significantly to FADD-dependent caspase-8 activation. A link between autophagy, FADD and caspase-8 activation was indeed reported previously during T cell expansion and cell cycle progression (27, 37), indicating that basal autophagy in proliferating T cells may establish low caspase-8 activities. Of note, autophagy and caspase-8 activity in these scenarios are a key physiological requirement for lymphocyte proliferation rather than inducing cell death (27, 31, 37). Protein degradation might quickly remove or restrict basal or naturally occurring sublethal levels of active caspase-8 in these cells. Proteasome inhibition instead, apart from enhancing caspase-8 activation through inducing autophagy, additionally may cause the stabilisation and abnormal accumulation of active caspase-8 through blocking protein degradation. This is likely to contribute to rendering autophagy-dependent caspase-8 activation to become potentially lethal.

Mechanistically, it was shown that caspase-8 and FADD can bind to Atg5/Atg12 clusters on autophagosomal membranes, which likely promotes caspase-8 activation through induced proximity (27). The necroptosis inducer and caspase-8 substrate RIPK1 was also reported to be a component of these complexes, however we could not find that RIPK1 activity contributed to cell death. This is consistent with the notion that RIPK1 only induces autophagy-dependent necroptosis when caspase-8 is absent (27). The late and zVAD-fmk sensitive loss in RIPK1 observed in our experiments indeed rather suggests that caspase-8 activation upon proteasome inhibition may actively suppress necroptotic responses.

We cannot rule out that apart from autophagosomes additional scaffolds for FADD-dependent caspase-8 activation are formed upon proteasome inhibition. Even though we could exclude that extrinsic stimulation of death receptors induced caspase-8 activation, it was shown previously that impaired protein degradation can result in an induction or abnormal accumulation of high-turnover death receptors (38). Such an accumulation may result in artificial death receptor oligomerisation and caspase-8 activation also in absence of death ligands. A recent study by Caro-Maldonado et al. published in this journal (39) showed that in response to glucose deprivation caspase-8 can be activated independent of death receptor signalling by an as of yet unresolved mechanism in cells incapable of activating the mitochondrial apoptosis pathway. Since protein degradation via the proteasome is a highly energy dependent process, lack of sufficient ATP as a consequence of glucose deprivation might promote the induction of autophagy and caspase-8 activation in a manner related to our observations.

Since most pro-apoptotic chemotherapeutics induce cell death via the mitochondrial pathway, elevated expression of Bcl-2 or other anti-apoptotic Bcl-2 family members poses a significant challenge to the development of efficient anti-cancer therapies. This is of clinical relevance since the expression of Bcl-2 or other antiapoptotic family members such as Bcl-xL or Mcl-1 has been associated with poor prognosis or increased risk of recurrence in various cancers, including for example chronic lymphocytic leukaemia, follicular lymphoma and early stage breast cancer (40-42). While Bcl-2 inhibiting compounds which re-sensitize cells to the mitochondrial pathway are currently in pre-clinical and clinical trials, no single compound is sufficient to antagonise all antiapoptotic family members with high efficiency or

without significant off-target effects (43). The direct activation of executioner caspases by caspase-8 offers the possibility to bypass the requirement for mitochondrial outer membrane permeabilisation for the induction of apoptosis execution, but in most cells is significantly impaired by the presence of XIAP, a major regulator of the caspase-8, -3 axis during extrinsically induced apoptosis (32, 44). We identified that the newly identified and death ligand-independent apical activation of caspase-8 in response to proteasome inhibition can be exploited to execute apoptosis in otherwise highly resistant Bcl-2 overexpressing cells when the function of XIAP is antagonised. This provides a new and attractive alternative strategy inducing cell death in cells otherwise not responsive to proapoptotic chemotherapeutics.

Materials and Methods

Reagents: Bortezomib was from Millennium Pharmaceuticals (Cambridge, MA, USA), Epoxomicin from Sigma-Aldrich (Dublin, Ireland) and MG-132 from Biomol (Plymouth Meeting, PA, USA). STS, CHX, tunicamycin and etoposide were purchased from Alexis (San Diego, CA, USA). z-Val-Ala-Asp(O-methyl)-fluoromethyl ketone (zVAD-fmk) was from Bachem (St Helen's, UK). Human recombinant TRAIL was from Leinco Technologies (St. Louis, MO, USA), human anti-Fas antibody was from (MBL, Caltag-Medystems, Buckinham, UK), TNF-α was from PeproTech EC Ltd (London, UK). Necrostatin-1, Pepstatin A, E64d and 3-methyl-adenine were purchased from Calbiochem/Merck (Nottingham, UK).

Peptide synthesis: A peptide comprised of an NH_2-terminal Smac-derived IAP antagonising sequence (AVPIAQK) and a COOH-terminal HIV-TAT protein-transduction domain (GRKKRRQRRRPPQ) (33) was prepared by standard solid phase peptide synthesis.

Cell Culture: Cells were cultivated in RPMI-1640 medium (Sigma-Aldrich) supplemented with 2 mM L-glutamine, 10% (v/v) heat-inactivated fetal bovine serum, 100 U/ml penicillin and 100 µg/ml streptomycin (Sigma-Aldrich) in a humidified atmosphere with 5% CO_2 at 37°C.

DNA and siRNA transfection: HeLa cells were transfected with pCFP-DEVD-YFP, pIMS-RP or pmCherry-GFP-LC3 plasmid DNA using Lipofectamine™ 2000 (Invitrogen, Paisley, UK) according to the manufactures instructions. siRNA

sequences known to specifically silence the expression of procaspase-3, procaspase-7, procaspase-8, FADD, XIAP, or Atg5 are listed in Supplemental material 1. siRNAs were transfected at a final concentration of 100 – 150 nM together with 800 ng pCFP-DEVD-YFP in 6 well plates. The relative timing of siRNA transfections prior to drug addition (24 hr for procaspase-3, -8, FADD, XIAP; 48 h for procaspase-7, Atg5) was optimized to achieve maximal protein depletion at a time of 24 h post bortezomib addition. The efficiency and maintenance of protein depletion in presence of bortezomib is shown in Supplemental Fig.8. Turbofect (Fermentas UK, York, UK) was used following the manufactures guidelines to transfect H460 or MCF-7 cells.

Immunoblotting: Cells were harvested and spun at 200 *g* for 3 min. Cell pellets were resuspended in SDS-lysis buffer (62.5 mM Tris-HCl, pH 6.8, 10 % (v/v) glycerin, 2 % (w/v) SDS, 1 mM phenylmethylsulfonyl fluoride, 1 µg/ml pepstatin A, 1 µg/ml leupeptin, and 5 µg/ml aprotinin) and incubated at 95°C for 20 min. Protein content was determined with the Micro BCA™ Protein Assay Kit (Thermo Scientific, Dublin, Ireland). Equal amounts of protein (20 µg) were run on SDS-polyacrylamide gels and subjected to immunoblotting as described before (21). Precision Plus Protein Standards (Bio-Rad, Munich, Germany) or PageRuler Prestained Portein Ladder Plus (Fermerntas, UK) molecular weight markers were used. A detailed list of antibodies used is provided in Supplemental material 1. Immunoblots were developed using the Immobilon™ Western Chemiluminescent HRP Substrate (Millipore, Molsheim, France). Chemiluminescence was detected at 12-bit dynamic range using a Fuji LAS 4000 CCD system (Fujifilm UK Ltd., Bedfordshire, UK).

Inhibition of the death receptor pathway: Human neutralizing antibodies against TRAIL-R1 and -R2 (ALX-522-004-C050 and ALX-522-005-C050), TNF-R1 (ALX-522-013-C050) and Fas (ALX-522-002-C050) were purchased from Enzo Life Sciences Ltd., Exeter, UK. Antibodies were added at a final concentration of 5 – 10 µg/ml two hours prior drug additions.

Flow cytometry: FRET flow cytometry was carried out using a Partec Cyflow ML16 flow cytometer (Partec, Münster, Germany) or a BD LSRII flow cytometer (Oxford, UK). Cells were re-suspended in ice-cold PBS and 10.000 gated events were acquired for each sample. Detailed settings for FRET flow cytometry and AnnexinV-FITC/propidium iodide (PI) cytometry as provided in Supplemental material 1. For Annexin-V/PI staining cells were trypsinised and incubated in binding buffer (10 mM HEPES, 140 mM NaCl, 2.5 mM $CaCl_2$) containing Annexin-V-FITC (5 µl/ml) (BioVision, Mountain View, CA, USA) and PI (2 µg/ml, Sigma-Aldrich) for 20 min at room temperature in the dark. Basic data acquisition in .fcs file format and analysis were performed using the Partec Flow Max (Partec, Münster, Germany) or Cyflogic (CyFlo Ltd, Turku, Finland) software. Ratiometric analysis of cellular fluorescence signals was performed using MATLAB (The Mathworks, UK) scripts developed in-house.

Fluorescence microscopy and digital imaging:

Cells were cultivated on 22 mm glass bottom dishes (Willco BV, Amsterdam, Netherlands). FRET probe fluorescence was observed using a Nikon Eclipse TE2000-S microscope equipped with a 40 x numerical aperture 1.3 oil immersion objective, and a dual camera adaptor (Nikon, MicronOptical, Enniscorthy, Ireland). Cells were

subjected to time lapse FRET imaging as described before (45). For the release of the MOMP reporter IMS-RP from the mitochondria into the cytosol, we analyzed the cellular fluorescence standard deviation from the average pixel intensity of individual cells (46). Compartmentalized IMS-RP contributes to a high s.d. The s.d. drops upon release of IMS-RP towards a homogeneous distribution throughout the cell. Baselines before the release were scaled to 100%. mCherry-GFP-LC3 fluorescence was observed using a Zeiss LSM710 confocal microscope. A detailed description of the imaging procedures is provided in Supplemental material 1.

Statistics:

Data are given as means + s.d. or s.e.m. For statistical comparison, Student's *t*-test or ANOVA followed by Tukey's test were used for normally distributed data. Otherwise, Mann-Whitney *U* test was used. *p* values smaller than 0.05 were considered to be statistically significant.

Acknowledgements:

This work was supported by grants from the Research Committee of the Royal College of Surgeons in Ireland, the Health Research Board Ireland (RP/2006/258; RP/2008/7) and Science Foundation Ireland (09/RFP/BIC2375) awarded to MR, the National Biophotonics and Imaging Platform Ireland (Higher Education Authority PRTLI Cycle 4) and the European Union (FP7 Health - APO-SYS). We are grateful to Dr. Douglas Green (St Jude Children's Research Hospital, Memphis), Dr. Frank Kruyt (University Medical Center Groningen), Drs. John Albeck and Peter Sorger (Harvard Medical School, Boston), Dr. Scott Oakes (University of California, San Francisco), Dr. Nathan Brady (German Cancer Research Center, Heidelberg), and Dr. Elaine Kay and Peter Jakob (Royal College of Surgeons in Ireland and Beaumont Hospital, Dublin) for the supply of cell lines, plasmids and additional materials. We also thank Eimear Costelloe, Kamil Jastrzebski and Dr. Tytus Bernas for technical assistance and helpful advice.

Conflict of interest: The authors declare no competing financial interests.

Note: Additional information is available as supplementary material.

Abbreviations List: 3-MA, 3-methyl adenine, bortezomib, [(1*R*)-3-methyl-1-({(2*S*)-3-phenyl-2-[(pyrazin-2-ylcarbonyl)amino]propanoyl}amino)butyl]boronic acid; CFP, cyan fluorescent protein; CHX, cycloheximide; epoxomicin, N-Acetyl-N-methyl-L-isoleucyl-L-isoleucyl-N-[(1S)-3-methyl-1-[[(2R)-2-methyloxiranyl]carbonyl]butyl]-L-threoninamide; FasL, fas ligand; FRET, Förster resonance energy transfer; MG-132, N-(benzyloxycarbonyl)leucinylleucinylleucinal; MOMP, mitochondrial outer

membrane permeabilisation; PBS, phosphate-buffered saline; PI, propidium iodide; IMS-RP, intermembrane-space reporter protein; STS, staurosporine; TMRM, tetramethylrhodamine methylester; TNF-α, tumour necrosis factor alpha; TRAIL, tumour necrosis factor-related apoptosis-inducing ligand; YFP, yellow fluorescent protein; zVAD, benzyloxycarbonyl-Val-Ala-Asp(*O*-methyl)-fluoromethylketone.

References

1. Carlucci A, Lignitto L, Feliciello A. Control of mitochondria dynamics and oxidative metabolism by cAMP, AKAPs and the proteasome. *Trends Cell Biol* 2008 Dec; **18** (12)**:** 604-613.

2. Jung T, Catalgol B, Grune T. The proteasomal system. *Mol Aspects Med* 2009 Aug; **30** (4)**:** 191-296.

3. Concannon CG, Koehler BF, Reimertz C, Murphy BM, Bonner C, Thurow N*, et al.* Apoptosis induced by proteasome inhibition in cancer cells: predominant role of the p53/PUMA pathway. *Oncogene* 2007 Mar 15; **26** (12)**:** 1681-1692.

4. Gomez-Bougie P, Wuilleme-Toumi S, Menoret E, Trichet V, Robillard N, Philippe M*, et al.* Noxa up-regulation and Mcl-1 cleavage are associated to apoptosis induction by bortezomib in multiple myeloma. *Cancer Res* 2007 Jun 1; **67** (11)**:** 5418-5424.

5. Luciano F, Jacquel A, Colosetti P, Herrant M, Cagnol S, Pages G*, et al.* Phosphorylation of Bim-EL by Erk1/2 on serine 69 promotes its degradation via the proteasome pathway and regulates its proapoptotic function. *Oncogene* 2003 Oct 2; **22** (43)**:** 6785-6793.

6. Marshansky V, Wang X, Bertrand R, Luo H, Duguid W, Chinnadurai G*, et al.* Proteasomes modulate balance among proapoptotic and antiapoptotic Bcl-2 family members and compromise functioning of the electron transport chain in leukemic cells. *J Immunol* 2001 Mar 1; **166** (5)**:** 3130-3142.

7. Brenner D, Mak TW. Mitochondrial cell death effectors. *Curr Opin Cell Biol* 2009 Dec; **21** (6)**:** 871-877.

8. Bhalla S, Balasubramanian S, David K, Sirisawad M, Buggy J, Mauro L*, et al.* PCI-24781 induces caspase and reactive oxygen species-dependent apoptosis through NF-kappaB mechanisms and is synergistic with bortezomib in lymphoma cells. *Clin Cancer Res* 2009 May 15; **15** (10)**:** 3354-3365.

9. Colado E, Alvarez-Fernandez S, Maiso P, Martin-Sanchez J, Vidriales MB, Garayoa M*, et al.* The effect of the proteasome inhibitor bortezomib on acute myeloid leukemia cells and drug resistance associated with the CD34+ immature phenotype. *Haematologica* 2008 Jan; **93** (1)**:** 57-66.

10. Li C, Li R, Grandis JR, Johnson DE. Bortezomib induces apoptosis via Bim and Bik up-regulation and synergizes with cisplatin in the killing of head and neck squamous cell carcinoma cells. *Mol Cancer Ther* 2008 Jun; **7** (6)**:** 1647-1655.

11. Tan TT, Degenhardt K, Nelson DA, Beaudoin B, Nieves-Neira W, Bouillet P*, et al.* Key roles of BIM-driven apoptosis in epithelial tumors and rational chemotherapy. *Cancer Cell* 2005 Mar; **7** (3)**:** 227-238.

12. Nikrad M, Johnson T, Puthalalath H, Coultas L, Adams J, Kraft AS. The proteasome inhibitor bortezomib sensitizes cells to killing by death receptor ligand TRAIL via BH3-only proteins Bik and Bim. *Mol Cancer Ther* 2005 Mar; **4** (3)**:** 443-449.

13. Sayers TJ, Brooks AD, Koh CY, Ma W, Seki N, Raziuddin A*, et al.* The proteasome inhibitor PS-341 sensitizes neoplastic cells to TRAIL-mediated apoptosis by reducing levels of c-FLIP. *Blood* 2003 Jul 1; **102** (1)**:** 303-310.

14. Ganten TM, Koschny R, Haas TL, Sykora J, Li-Weber M, Herzer K*, et al.* Proteasome inhibition sensitizes hepatocellular carcinoma cells, but not human hepatocytes, to TRAIL. *Hepatology* 2005 Sep; **42** (3)**:** 588-597.

15. Hallett WH, Ames E, Motarjemi M, Barao I, Shanker A, Tamang DL*, et al.* Sensitization of tumor cells to NK cell-mediated killing by proteasome inhibition. *J Immunol* 2008 Jan 1; **180** (1)**:** 163-170.

16. Galban S, Duckett CS. XIAP as a ubiquitin ligase in cellular signaling. *Cell Death Differ* 2010 Jan; **17** (1)**:** 54-60.

17. Vaux DL, Silke J. IAPs, RINGs and ubiquitylation. *Nat Rev Mol Cell Biol* 2005 Apr; **6** (4)**:** 287-297.

18. Rehm M, Dussmann H, Prehn JH. Real-time single cell analysis of Smac/DIABLO release during apoptosis. *J Cell Biol* 2003 Sep 15; **162** (6)**:** 1031-1043.

19. Fernandes-Alnemri T, Armstrong RC, Krebs J, Srinivasula SM, Wang L, Bullrich F*, et al.* In vitro activation of CPP32 and Mch3 by Mch4, a novel human apoptotic cysteine protease containing two FADD-like domains. *Proc Natl Acad Sci U S A* 1996 Jul 23; **93** (15)**:** 7464-7469.

20. Zhang XD, Gillespie SK, Hersey P. Staurosporine induces apoptosis of melanoma by both caspase-dependent and -independent apoptotic pathways. *Mol Cancer Ther* 2004 Feb; **3** (2)**:** 187-197.

21. Rehm M, Dussmann H, Janicke RU, Tavare JM, Kogel D, Prehn JH. Single-cell fluorescence resonance energy transfer analysis demonstrates that caspase activation during apoptosis is a rapid process. Role of caspase-3. *J Biol Chem* 2002 Jul 5; **277** (27)**:** 24506-24514.

22. McStay GP, Salvesen GS, Green DR. Overlapping cleavage motif selectivity of caspases: implications for analysis of apoptotic pathways. *Cell Death Differ* 2008 Feb; **15** (2)**:** 322-331.

23. Rehm M, Huber HJ, Dussmann H, Prehn JH. Systems analysis of effector caspase activation and its control by X-linked inhibitor of apoptosis protein. *Embo J* 2006 Sep 20; **25** (18)**:** 4338-4349.

24. Dussmann H, Rehm M, Kogel D, Prehn JH. Outer mitochondrial membrane permeabilization during apoptosis triggers caspase-independent mitochondrial and caspase-dependent plasma membrane potential depolarization: a single-cell analysis. *J Cell Sci* 2003; **116** (Pt 3)**:** 525-536.

25. Hughes MA, Harper N, Butterworth M, Cain K, Cohen GM, MacFarlane M. Reconstitution of the death-inducing signaling complex reveals a substrate switch that determines CD95-mediated death or survival. *Mol Cell* 2009 Aug 14; **35** (3)**:** 265-279.

26. Pandey UB, Nie Z, Batlevi Y, McCray BA, Ritson GP, Nedelsky NB*, et al.* HDAC6 rescues neurodegeneration and provides an essential link between autophagy and the UPS. *Nature* 2007 Jun 14; **447** (7146)**:** 859-863.

27. Bell BD, Leverrier S, Weist BM, Newton RH, Arechiga AF, Luhrs KA*, et al.* FADD and caspase-8 control the outcome of autophagic signaling in proliferating T cells. *Proc Natl Acad Sci U S A* 2008 Oct 28; **105** (43)**:** 16677-16682.

28. Kuusisto E, Suuronen T, Salminen A. Ubiquitin-binding protein p62 expression is induced during apoptosis and proteasomal inhibition in neuronal cells. *Biochem Biophys Res Commun* 2001 Jan 12; **280** (1)**:** 223-228.

29. Pankiv S, Clausen TH, Lamark T, Brech A, Bruun JA, Outzen H*, et al.* p62/SQSTM1 binds directly to Atg8/LC3 to facilitate degradation of ubiquitinated protein aggregates by autophagy. *J Biol Chem* 2007 Aug 17; **282** (33)**:** 24131-24145.

30. Yu L, Alva A, Su H, Dutt P, Freundt E, Welsh S*, et al.* Regulation of an ATG7-beclin 1 program of autophagic cell death by caspase-8. *Science* 2004 Jun 4; **304** (5676)**:** 1500-1502.

31. Ch'en IL, Beisner DR, Degterev A, Lynch C, Yuan J, Hoffmann A*, et al.* Antigen-mediated T cell expansion regulated by parallel pathways of death. *Proc Natl Acad Sci U S A* 2008 Nov 11; **105** (45)**:** 17463-17468.

32. Jost PJ, Grabow S, Gray D, McKenzie MD, Nachbur U, Huang DC*, et al.* XIAP discriminates between type I and type II FAS-induced apoptosis. *Nature* 2009 Aug 20; **460** (7258)**:** 1035-1039.

33. Fulda S, Wick W, Weller M, Debatin KM. Smac agonists sensitize for Apo2L/TRAIL- or anticancer drug-induced apoptosis and induce regression of malignant glioma in vivo. *Nat Med* 2002 Aug; **8** (8)**:** 808-815.

34. Miller CP, Ban K, Dujka ME, McConkey DJ, Munsell M, Palladino M*, et al.* NPI-0052, a novel proteasome inhibitor, induces caspase-8 and ROS-

dependent apoptosis alone and in combination with HDAC inhibitors in leukemia cells. *Blood* 2007 Jul 1; **110** (1)**:** 267-277.

35. Liu X, Yue P, Chen S, Hu L, Lonial S, Khuri FR*, et al.* The Proteasome Inhibitor PS-341 (Bortezomib) Up-Regulates DR5 Expression Leading to Induction of Apoptosis and Enhancement of TRAIL-Induced Apoptosis Despite Up-Regulation of c-FLIP and Survivin Expression in Human NSCLC Cells. *Cancer Research* 2007; **67** (10)**:** 4981-4988.

36. Boatright KM, Renatus M, Scott FL, Sperandio S, Shin H, Pedersen IM*, et al.* A unified model for apical caspase activation. *Mol Cell* 2003 Feb; **11** (2)**:** 529-541.

37. Arechiga AF, Bell BD, Leverrier S, Weist BM, Porter M, Wu Z*, et al.* A Fas-associated death domain protein/caspase-8-signaling axis promotes S-phase entry and maintains S6 kinase activity in T cells responding to IL-2. *J Immunol* 2007 Oct 15; **179** (8)**:** 5291-5300.

38. Voortman J, Resende TP, Abou El Hassan MAI, Giaccone G, Kruyt FAE. TRAIL therapy in non–small cell lung cancer cells: sensitization to death receptor–mediated apoptosis by proteasome inhibitor bortezomib. *Molecular Cancer Therapeutics* 2007; **6** (7)**:** 2103-2112.

39. Caro-Maldonado A, Tait SW, Ramirez-Peinado S, Ricci JE, Fabregat I, Green DR*, et al.* Glucose deprivation induces an atypical form of apoptosis mediated by caspase-8 in Bax-, Bak-deficient cells. *Cell Death Differ* 2010 Mar 5.

40. Pepper C, Lin TT, Pratt G, Hewamana S, Brennan P, Hiller L*, et al.* Mcl-1 expression has in vitro and in vivo significance in chronic lymphocytic leukemia and is associated with other poor prognostic markers. *Blood* 2008 Nov 1; **112** (9)**:** 3807-3817.

41. Zhao WL, Daneshpouy ME, Mounier N, Briere J, Leboeuf C, Plassa LF*, et al.* Prognostic significance of bcl-xL gene expression and apoptotic cell counts in follicular lymphoma. *Blood* 2004 Jan 15; **103** (2)**:** 695-697.

42. Yang Q, Moran MS, Haffty BG. Bcl-2 expression predicts local relapse for early-stage breast cancer receiving conserving surgery and radiotherapy. *Breast Cancer Res Treat* 2009 May; **115** (2)**:** 343-348.

43. Vogler M, Dinsdale D, Dyer MJ, Cohen GM. Bcl-2 inhibitors: small molecules with a big impact on cancer therapy. *Cell Death Differ* 2009 Mar; **16** (3)**:** 360-367.

44. Wilson TR, McEwan M, McLaughlin K, Le Clorennec C, Allen WL, Fennell DA*, et al.* Combined inhibition of FLIP and XIAP induces Bax-independent apoptosis in type II colorectal cancer cells. *Oncogene* 2009 Jan 8; **28** (1)**:** 63-72.

45. Hellwig CT, Kohler BF, Lehtivarjo AK, Dussmann H, Courtney MJ, Prehn JH*, et al.* Real time analysis of tumor necrosis factor-related apoptosis-inducing ligand/cycloheximide-induced caspase activities during apoptosis initiation. *J Biol Chem* 2008 Aug 1; **283** (31)**:** 21676-21685.

46. Flanagan L, Sebastia J, Tuffy LP, Spring A, Lichawska A, Devocelle M*, et al.* XIAP impairs Smac release from the mitochondria during apoptosis. *Cell Death and Dis* 2010; **1:** e49.

Titles and Legends to Figures

Fig.1: Proteasome inhibition promotes residual processing of procaspase-3 in cells expressing high levels of Bcl-2.

(A) Proteasome inhibition induces residual procaspase-3 processing in Bcl-2 overexpressing HeLa cells. Parental and Bcl-2 overexpressing HeLa cells were compared by Western blotting for processing of procaspase-3 in response to 1 μM STS (8 h), 100 nM bortezomib (32 h), 3 μM tunicamycin (32 h), or 10 μM etoposide (32 h). Arrows indicate p20 and p19 caspase-3 subunits found in HeLa-Bcl-2 cells due to residual procaspase-3 processing. Fully mature p17 subunits could not be detected in HeLa-Bcl-2 cells. β-actin served as loading control. **(B-D)** Procaspase-3 processing in response to 100 nM bortezomib, 50 nM epoxomicin or 5 μM MG-132 was compared between parental and Bcl-2 overexpressing HeLa cells. While p20 and p19 subunits could be detected, fully mature caspase-3 (p17) was not detected in HeLa-Bcl-2 cells. 50 μM pan-caspase inhibitor zVAD-fmk was used in combination with proteasome inhibitors in additional controls. β-actin served as loading control. **(E)** Procaspase-3 processing in response to 100 nM bortezomib was analysed in parental and Bcl-2 overexpressing H460 cells. Arrows indicate p20, p19 and p17 subunits. α-tubulin served as loading control. **(F)** As in (E), procaspase-3 processing in response to 100 nM bortezomib was analysed in parental or Bax/Bak deficient mouse embryonic fibroblasts. Porin served as loading control. **(G-I)** Cell death in response to 100 nM bortezomib was determined by propidium iodide staining. Bcl-2 overexpression or Bax/Bak deficiency significantly reduced cell death. 50 μM zVAD-fmk was added in additional control groups. Data are shown as means +/- s.d.

Asterisks indicate significant reduction in cell death ($p<0.05$, Student's t-test). All experiments were preformed three times with comparable results.

Fig.2: Proteasome inhibition induces low levels of DEVDase activity in Bcl-2 over-expressing cells.

(A) A CFP-DEVD-YFP FRET probe was used to measure DEVDase activity in individual cells by flow cytometry. Cleavage of the probe by DEVDases results in a loss in FRET and a concomitant increase in CFP emission. **(B)** Flow cytometric analysis of parental HeLa cells expressing the DEVD FRET probe. Cells were treated for the indicated times with 100 nM bortezomib. zVAD-fmk co-treated controls ensured caspase-specificity of the readout. For comparison, control groups treated with 1 μM STS (8 h) are shown as well. Data are means + s.d. from n = 3 experiments. Asterisks indicate significant increase in FRET probe cleavage above control groups ($p<0.05$; one way ANOVA and subsequent Tukey's test). **(C)** Flow cytometric analysis of HeLa-Bcl-2 cells expressing the DEVD FRET probe. Cells were treated as in (B). Data are means + s.d. from n = 3 experiments. Asterisks indicate significant increase in FRET probe cleavage above control groups ($p<0.05$; one way ANOVA and subsequent Tukey's test). **(D)** As described in (B,C), DEVD FRET probe cleavage was analysed in wild type and Bax/Bak-deficient mouse embryonic fibroblasts. **(E)** Scatter plots displaying DEVD FRET probe cleavage in parental HeLa cells. Treatment with 100 nM bortezomib resulted in clearly separable populations of cells with intact or cleaved FRET probe. Caspase inhibition by zVAD-fmk inhibited probe cleavage. **(F)** Scatter plots displaying DEVD FRET probe cleavage in HeLa-Bcl-2 cells. Following treatment with 100 nM bortezomib populations of cells with intact or cleaved FRET probe were inseparable, indicating

slow or incomplete substrate cleavage. Caspase inhibition by zVAD-fmk inhibited probe cleavage. **(G, H)** Ratiometric analysis of FRET probe cleavage indicates that bortezomib-induced DEVDase activity in parental HeLa cells (G) resulted in separated peaks of intact or cleaved probe. In comparison, probe cleavage was significantly reduced in HeLa-Bcl-2 cells (H), as indicated by a right-shift and reduction in peak height at 24 h and inseparable peaks at 48 h post addition of 100 nM bortezomib.

Fig.3: Time-lapse analysis of DEVDase activation and activity induced by proteasome inhibition.

(A) Parental and Bcl-2 overexpressing cells were analysed for DEVDase activation in FRET imaging experiments. The incidence of DEVDase activation following treatment with 100 nM bortezomib was determined from the total number of cells analysed (n = 43 parental cells from 4 experiments and n = 27 Bcl-2 overexpressing cells from 6 experiments). DEVDase activation was evaluated as an irreversible increase of the CFP/YFP ratio signal above the baseline. Bcl-2 overexpression did not affect the frequency of DEVDase activation. **(B)** The time from bortezomib addition until activation of DEVDases was determined for all cells measured. DEVDase activity was detected later in Bcl-2 overexpressing cells. Asterisk indicates significant difference ($p<0.05$, *U*-test). **(C)** The duration of DEVD probe cleavage was determined for all cells analysed. Bcl-2 overexpression prolonged the duration of probe cleavage. Asterisk indicates significant difference ($p<0.05$, *U*-test). **(D)** The DEVDase activity was determined as the rate of probe cleavage (change in CFP/YFP emission over time) for all cells investigated. Overexpression of Bcl-2 strongly reduced the DEVDase activity determined in single living cells. Asterisk indicates

significant difference ($p<0.05$, *U*-test). **(E)** DEVD FRET probe cleavage in parental HeLa cells. Traces of DEVD FRET probe cleavage are shown for four representative HeLa cells following exposure to 100 nM bortezomib. FRET probe cleavage resulted in an increase in the CFP/YFP emission ratio. Onset of DEVDase activity was set to time zero. TMRM fluorescence was plotted to indicate changes in mitochondrial membrane potentials. Mitochondrial depolarisation started shortly before DEVDase activation. Similar results were obtained from n = 23 additional cells. **(F)** DEVD FRET probe cleavage in HeLa cells overexpressing Bcl-2. Experimental traces of DEVD FRET probe cleavage are shown for four representative HeLa-Bcl-2 cells following exposure to 100 nM bortezomib. Onset of DEVDase activity was set to time zero. FRET probe cleavage displayed in increases in the CFP/YFP emission ratio that were lower and prolonged when compared to parental HeLa cells (see **E**). In contrast to parental HeLa cells, changes in mitochondrial membrane potentials were not detectable at the time DEVDase activation was measured. Late changes in TMRM signals resulted from cells rounding up and detaching. Similar results were obtained for n = 12 additional cells. **(G)** DEVD FRET probe cleavage in parental HeLa cells was observed in parallel with the release of red fluorescent protein (mCherry) from the mitochondrial intermembrane space (IMS-RP). The release of IMS-RP results in a fluorescence re-distribution towards a homogeneous signal across the cell (see also methods section). The start of IMS-RP release was therefore defined as the time at which the cellular fluorescence s.d. started to drop. IMS-RP release preceded DEVDase activation. Similar results were obtained from n = 5 additional cells. **(H)** In HeLa cells overexpressing Bcl-2, DEVDase activation resulted in slow and prolonged substrate cleavage. No release of IMS-RP could be detected, indicating that DEVDase activity was established independent of MOMP. Similar results were obtained for n =

14 cells. **(I)** α-spectrin cleavage after bortezomib treatment. Prolonged exposure to bortezomib resulted in the detection of the caspase-specific 120 kDa cleavage product and loss of full length α-spectrin in parental cells, which was strongly diminished in HeLa cells overexpressing Bcl-2. α-tubulin served as loading control.

Fig.4: DEVDase activity in response to proteasome inhibition does not arise from caspase-3 or -7 activity.

(A) Depletion of procaspase-3 by siRNA transfection. HeLa-Bcl-2 cells were analysed for procaspase-3 expression at the indicated times following siRNA transfection. β-actin served as loading control. A scrambled siRNA (scr) was transfected in control cells. **(B)** HeLa-Bcl-2 cells depleted of procaspase-3 expression were analysed for DEVD FRET probe cleavage by flow cytometry following treatment with 100 nM bortezomib. siRNA transfection preceded drug addition by 24 h to provide efficient target depletion 24 h subsequent to bortezomib addition (see Supplemental Fig.8). Depletion of caspase-3 did not reduce FRET probe cleavage. Bars display changes in FRET substrate cleavage [%] above untreated controls. Data represent mean + s.d. from n = 9 values obtained from bootstrap-resampling of independent treatment and control triplicates. Experiment was repeated with similar results. **(C)** Depletion of procaspase-7 by siRNA transfection in Bcl-2 overexpressing MCF-7 cells. Cells were analysed for procaspase-7 expression at the indicated times following siRNA transfection. β-actin served as loading control. Scrambled siRNA (scr) was transfected in control cells. **(D)** MCF-7-Bcl-2 cells depleted of procaspase-7 and expressing the DEVD FRET probe were exposed to 100 nM bortezomib for 48 h and analysed by flow cytometry. siRNA transfection preceded drug addition by 48 h to provide efficient target depletion 24 h subsequent to bortezomib addition (see

Supplemental Fig.8). A continuous spectrum of substrate cleavage which could not be inhibited by procaspase-7 depletion was detected. Experiment was repeated with similar results.

Fig.5: DEVDase activity in response to proteasome inhibition arises from FADD-dependent caspase-8 activation.

(A) Time resolved analysis of procaspase-8 processing into p43/41 and p18 subunits induced by 100 nM bortezomib in parental HeLa cells. Porin served as loading control. **(B)** As in (A), procaspase-8 processing was investigated in HeLa cells overexpressing Bcl-2. Procaspase-8 was only residually processed (arrows) and processing occurred at later times than in parental HeLa cells. Porin served as loading control. All experiments were preformed three times with comparable results. **(C)** Bid processing was observed by Western blotting in whole cell extract of HeLa or HeLa Bcl-2 cells treated with 100 nM bortezomib for the indicated times. Corresponding to data on caspase-8 processing (A,B), Bid cleavage in HeLa Bcl-2 cells was delayed. Arrow and high contrast panel indicate truncated Bid. Porin served as loading control. **(D)** Depletion of caspase-8 by siRNA transfection. HeLa-Bcl-2 cells were analysed for procaspase-8 expression at the indicated times following siRNA transfection. β-actin served as loading control. A scrambled siRNA (scr) was transfected in control cells. **(E)** HeLa Bcl-2 cells depleted of procaspase-8 expression were analysed for DEVD FRET probe cleavage by flow cytometry following treatment with 100 nM bortezomib. siRNA transfection preceded drug addition by 24 h to provide efficient target depletion 24 h subsequent to bortezomib addition (see Supplemental Fig.8). Bars display changes in FRET substrate cleavage [%] above untreated controls. Data represent mean + s.d. from n = 9 values obtained from bootstrap-resampling of

independent triplicates. Depletion of procaspase-8 significantly reduced FRET probe cleavage ($p<0.05$, *U*-test). Experiment was repeated with similar results. **(F)** Procaspase-8 depletion by siRNA delivery impairs DEVDase activation in HeLa Bcl-2 cells after exposure to bortezomib. After depletion of procaspase-3 or -8 cells were analysed for DEVDase activation by time lapse FRET imaging. Scrambled siRNA was transfected in control cells. Procaspase-8 depletion resulted in significantly less cells displaying DEVDase activity. Data are from n = 27 (scr), 27 (procaspase-3) and 40 (procaspase-8) cells from 3 – 4 independent experiments per group. **(G)** Depletion of procaspase-8 reduced caspase-3 processing as evidenced by a lower conversion of procaspase-3 into p20/p19 subunits. HeLa Bcl-2 cells were treated with 100 nM bortezomib for 48 hrs. α-tubulin served as loading control. **(H)** Cell death in response to 100 nM bortezomib was determined by propidium iodide staining. Depletion of procaspase-8 significantly reduced cell death. siRNA transfection preceded drug addition by 24 h to provide efficient target depletion 24 h subsequent to bortezomib addition (see Supplemental Fig.8). Data are shown as means +/- s.d., asterisks indicate significant differences ($p<0.05$, Student's t-test). **(I)** Depletion of FADD by siRNA transfection. As in (D), HeLa-Bcl-2 cells were analysed for FADD expression at the indicated times following siRNA transfection. **(J)** As in (E), HeLa Bcl-2 cells depleted of FADD expression with 100 nM FADD siRNA were analysed for DEVD FRET probe cleavage by flow cytometry following treatment with 100 nM bortezomib. siRNA transfection preceded drug addition by 24 h to provide efficient target depletion 24 h subsequent to bortezomib addition (see Supplemental Fig.8). Bars display changes in FRET substrate cleavage [%] above untreated controls. Data represent mean + s.d. from n = 9 values obtained from bootstrap-resampling of

independent triplicates. Depletion of FADD significantly reduced FRET probe cleavage ($p<0.05$, U-test). Experiment was repeated with similar results.

Fig.6: Apical caspase-8 activation in response to proteasome inhibition is independent of death receptor ligands.

(A) Neutralisation of the extrinsic pathway in parental HeLa cells. 2 h pre-treatment with 5 µg/ml TRAIL-R1:Fc + 5 µg/ml TRAIL-R2:Fc, 5 µg/ml TNF-R1:Fc or 10 µg/ml Fas:Fc antibodies, respectively, completely abolished extrinsically induced caspase-3 processing. Cells were treated for 6 h with 10 ng/ml TRAIL plus 1 µg/ml CHX or 100 ng/ml FasL plus 1 µg/ml CHX or for 8 h with 100 ng/ml TNF-α plus 1 µg/ml CHX. α-tubulin served as loading control. **(B)** Inhibition of death receptors did not diminish submaximal procaspase-3 processing in response to proteasome inhibition in HeLa-Bcl-2 cells. Cells were pre-treated as in (A), and subsequently exposed to 100 nM bortezomib for 32 h or 48 h. α-tubulin served as loading control. **(C)** Procaspase-8 and -3 processing was investigated when using a combination of all neutralizing antibodies. β-actin served as loading control.

Fig.7: Autophagy strongly contributes to caspase-8 processing in response to proteasome inhibition.

(A) Whole cell extracts of HeLa Bcl-2 cells treated with 100 nM bortezomib for 32 h in presence or absence of inhibitors of lysosomal proteases were probed for LC3 and p62. Asterisk indicates an unspecific band. β-actin served as loading control. **(B)** Whole cell extracts of HeLa Bcl-2 cells treated with 100 nM bortezomib for the indicated times were probed for the accumulation of p62, FADD or RIPK1. Porin served as loading control. **(C)** HeLa Bcl-2 cells expressing an mCherry-GFP-LC3

fusion protein were analysed for the induction of autophagy subsequent to addition of 100 nM bortezomib by confocal microscopy. GFP punctae represent autophagosomes, mCherry punctae represent both autophagosomes and autolysosomes. **(D)** Procaspase-8 processing and LC3 accumulation and conversion was analysed in HeLa Bcl-2 cells treated with 5 mM 3-MA, 10 μM necrostatin, 50 nM botezomib or combinations thereof for 32 h. 3-MA significantly reduced bortezomib-induced procaspase-8 processing and LC3-I to LC3-II conversion. β-actin served as loading control. **(E)** Cell death of HeLa Bcl-2 cells in response to treatments as in (D) was determined by propidium iodide staining. Data are shown as means +/- s.d from n=3 parallel independent cultures. Asterisk indicates significant difference ($p<0.05$, Student's t-test). Experiment was repeated with similar results. **(F)** Atg5 depletion blocks procaspase-8 processing. Atg5 was depleted in HeLa Bcl-2 cells using shRNA transfection. 48 h subsequent to transfection cells were exposed to 50 nM bortezomib for 40 h. Whole cell lysates were analysed for the amount of Atg12-Atg5 conjugates, LC3-I accumulation and conversion to LC3-II, and procaspase-8 processing. β-actin served as loading control. **(G)** Cell death of HeLa Bcl-2 cells in response to treatments as in (F) was determined by propidium iodide staining. Data are shown as means +/- s.d from n=3 parallel independent cultures. Asterisk indicates significant difference ($p<0.05$, Student's t-test). All experiments were repeated at least once and similar results were obtained.

Fig.8: XIAP depletion and Smac-derived XIAP antagonising peptides enhance proteasome inhibitor-induced DEVDase activation and apoptosis in Bcl-2 overexpressing cells.

(A) Depletion of XIAP by siRNA transfection. HeLa-Bcl-2 cells were analysed for XIAP expression at the indicated times following siRNA transfection. Asterisk indicates an unspecific band. β-actin served as loading control. A scrambled siRNA (scr) was transfected in control cells. **(B)** HeLa Bcl-2 cells depleted of XIAP expression were analysed for DEVD FRET probe cleavage by flow cytometry following treatment with 100 nM bortezomib. siRNA transfection preceded drug addition by 24 h to provide efficient target depletion 24 h subsequent to bortezomib addition (see Supplemental Fig.8). Depletion of XIAP significantly enhanced FRET probe cleavage. Data represent mean + s.d. from n = 9 values obtained from bootstrap-resampling of independent treatment and control triplicates. Experiment was repeated with similar results. **(C)** Cell death in response to 100 nM bortezomib was determined by propidium iodide staining. Depletion of XIAP significantly enhanced cell death following treatment of HeLa Bcl-2 cells with 100 nM bortezomib. Data are shown as means +/- s.d., asterisks indicate significant differences ($p<0.05$, Student's t-test). **(D)** Smac-derived XIAP antagonising AVPIA peptides enhance apoptosis execution in response to proteasome inhibition in HeLa Bcl-2 cells. Apoptotic cell death was measured by flow cytometry using AnnexinV-FITC and propidium iodide staining. Mild responses were detected following proteasome inhibition by bortezomib (100 nM, 32 h). Addition of AVPIA peptide (100 μM) significantly enhanced cell death. Untreated cells or cells receiving only AVPIA peptide did not undergo apoptosis execution. Experiment was repeated with similar results. **(E)** As in (D) H460 cells overexpressing Bcl-2 were exposed to bortezomib, AVPIA peptide or both. Co-treatment strongly enhanced cell death following 32 h of treatment. Experiment was repeated with similar results.

Fig.1

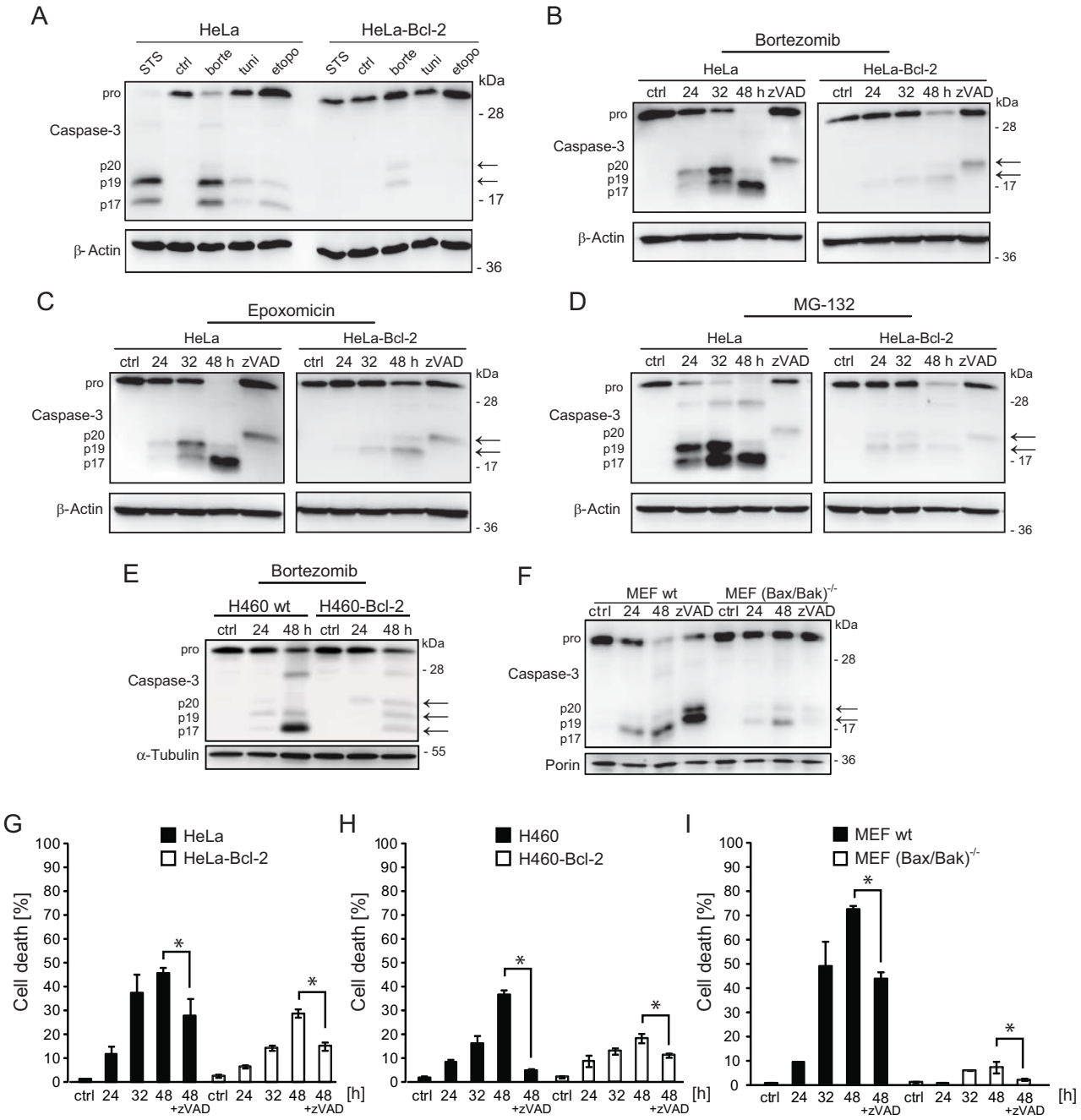
A
HeLa
HeLa-Bcl-2
STS
ctrl
borte
tuni
etopo
kDa
pro
Caspase-3
p20
p19
p17
β-Actin
- 28
- 17
- 36
B
Bortezomib
HeLa
HeLa-Bcl-2
ctrl 24 32 48 h zVAD
C
Epoxomicin
D
MG-132
E
Bortezomib
H460 wt
H460-Bcl-2
ctrl 24 48 h
α-Tubulin
- 55
F
MEF wt
MEF (Bax/Bak)-/-
ctrl 24 48 zVAD
Porin
G
HeLa
HeLa-Bcl-2
Cell death [%]
ctrl 24 32 48 48 +zVAD
[h]
H
H460
H460-Bcl-2
I
MEF wt
MEF (Bax/Bak)-/-

Fig.2

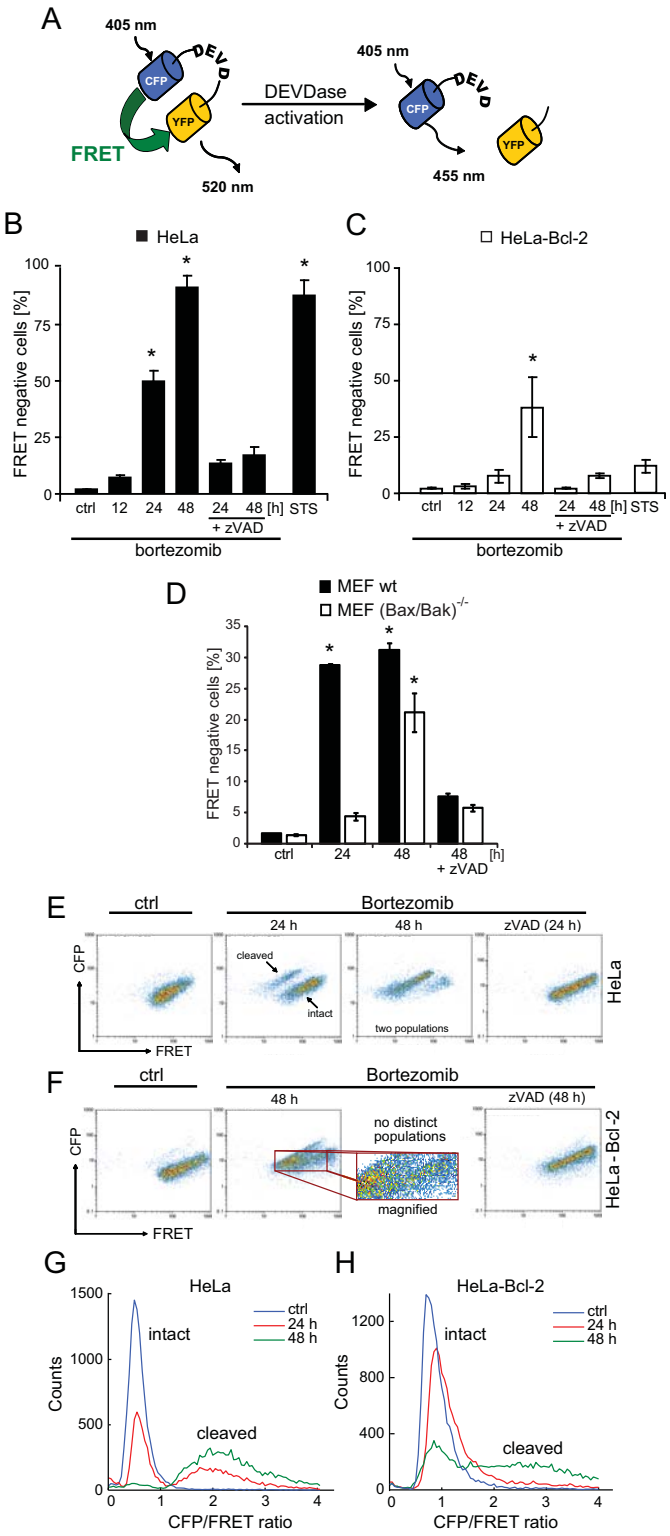
A
405 nm
CFP
DEVD
YFP
FRET
520 nm
DEVDase
activation
405 nm
CFP
DEVD
YFP
455 nm
B
HeLa
FRET negative cells [%]
100
75
50
25
0
ctrl
12
24
48
24
48 [h]
STS
+ zVAD
bortezomib
C
HeLa-Bcl-2
FRET negative cells [%]
ctrl
12
24
48
24
48 [h]
STS
+ zVAD
bortezomib
D
MEF wt
MEF (Bax/Bak)-/-
FRET negative cells [%]
35
30
25
20
15
10
5
0
ctrl
24
48
48
[h]
+ zVAD
E
ctrl
Bortezomib
24 h
48 h
zVAD (24 h)
CFP
FRET
cleaved
intact
two populations
HeLa
F
ctrl
Bortezomib
48 h
zVAD (48 h)
CFP
FRET
no distinct
populations
magnified
HeLa - Bcl-2
G
HeLa
ctrl
24 h
48 h
intact
cleaved
Counts
1500
1000
500
0
0
1
2
3
4
CFP/FRET ratio
H
HeLa-Bcl-2
ctrl
24 h
48 h
intact
cleaved
Counts
1200
800
400
0
0
1
2
3
4
CFP/FRET ratio

Fig.3

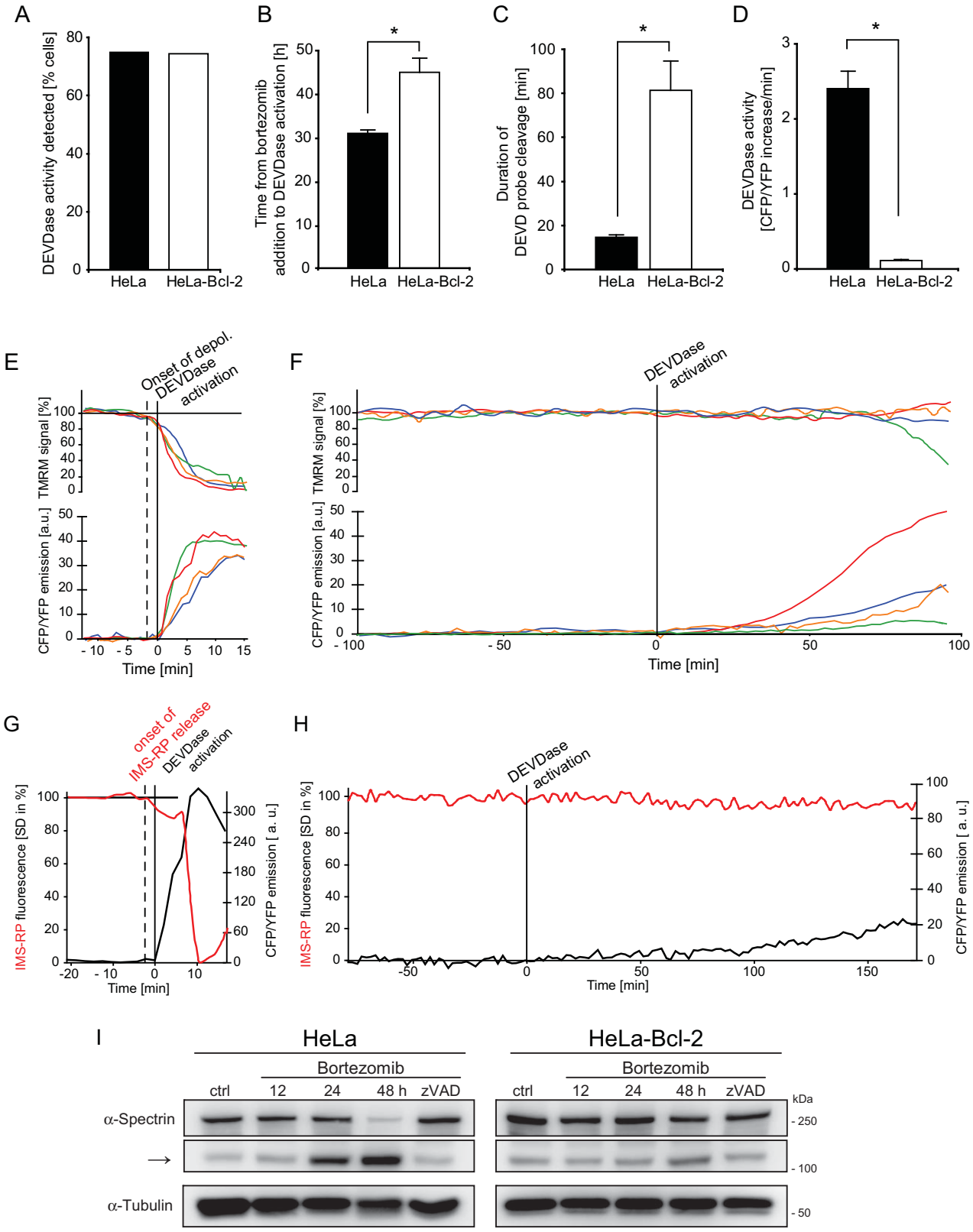
A
DEVDase activity detected [% cells]
HeLa
HeLa-Bcl-2
B
Time from bortezomib addition to DEVDase activation [h]
C
Duration of DEVD probe cleavage [min]
D
DEVDase activity [CFP/YFP increase/min]
E
Onset of depol.
DEVDase activation
TMRM signal [%]
CFP/YFP emission [a.u.]
Time [min]
F
DEVDase activation
G
onset of IMS-RP release
DEVDase activation
IMS-RP fluorescence [SD in %]
CFP/YFP emission [a. u.]
H
I
HeLa
HeLa-Bcl-2
Bortezomib
ctrl
12
24
48 h
zVAD
kDa
α-Spectrin
α-Tubulin
- 250
- 100
- 50

Fig.4

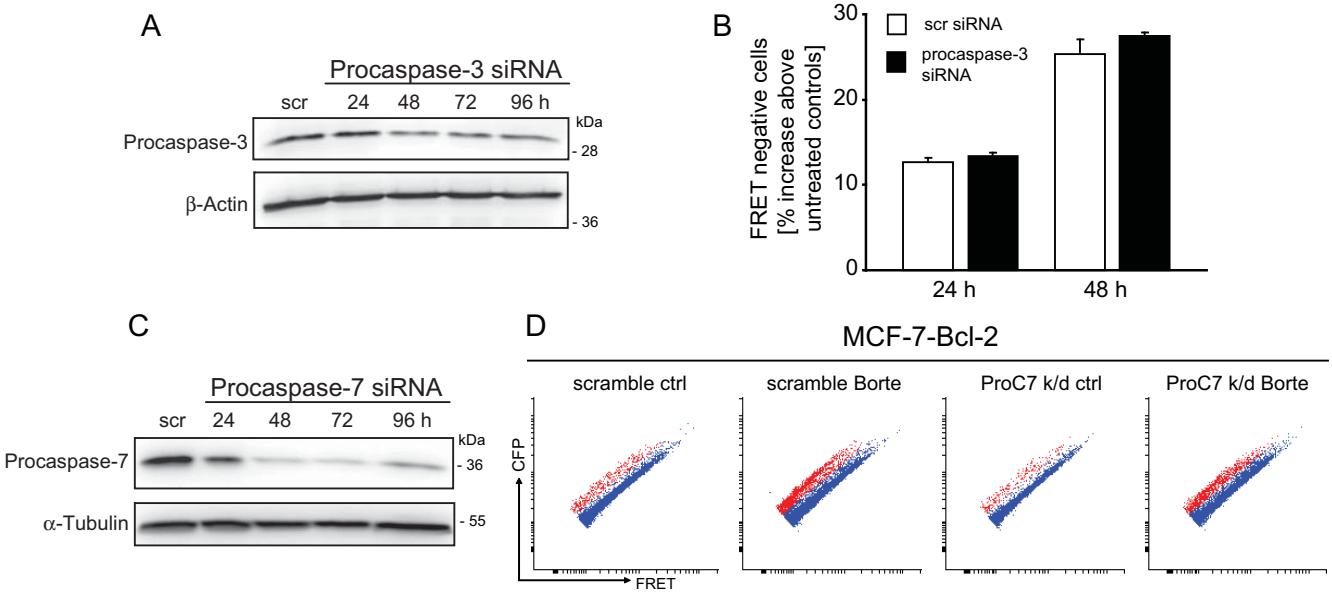
A
Procaspase-3 siRNA
scr
24
48
72
96 h
kDa
Procaspase-3
- 28
β-Actin
- 36
B
FRET negative cells
[% increase above
untreated controls]
30
20
10
0
scr siRNA
procaspase-3
siRNA
24 h
48 h
C
Procaspase-7 siRNA
scr
24
48
72
96 h
kDa
Procaspase-7
- 36
α-Tubulin
- 55
D
MCF-7-Bcl-2
scramble ctrl
scramble Borte
ProC7 k/d ctrl
ProC7 k/d Borte
CFP
FRET

Fig.5

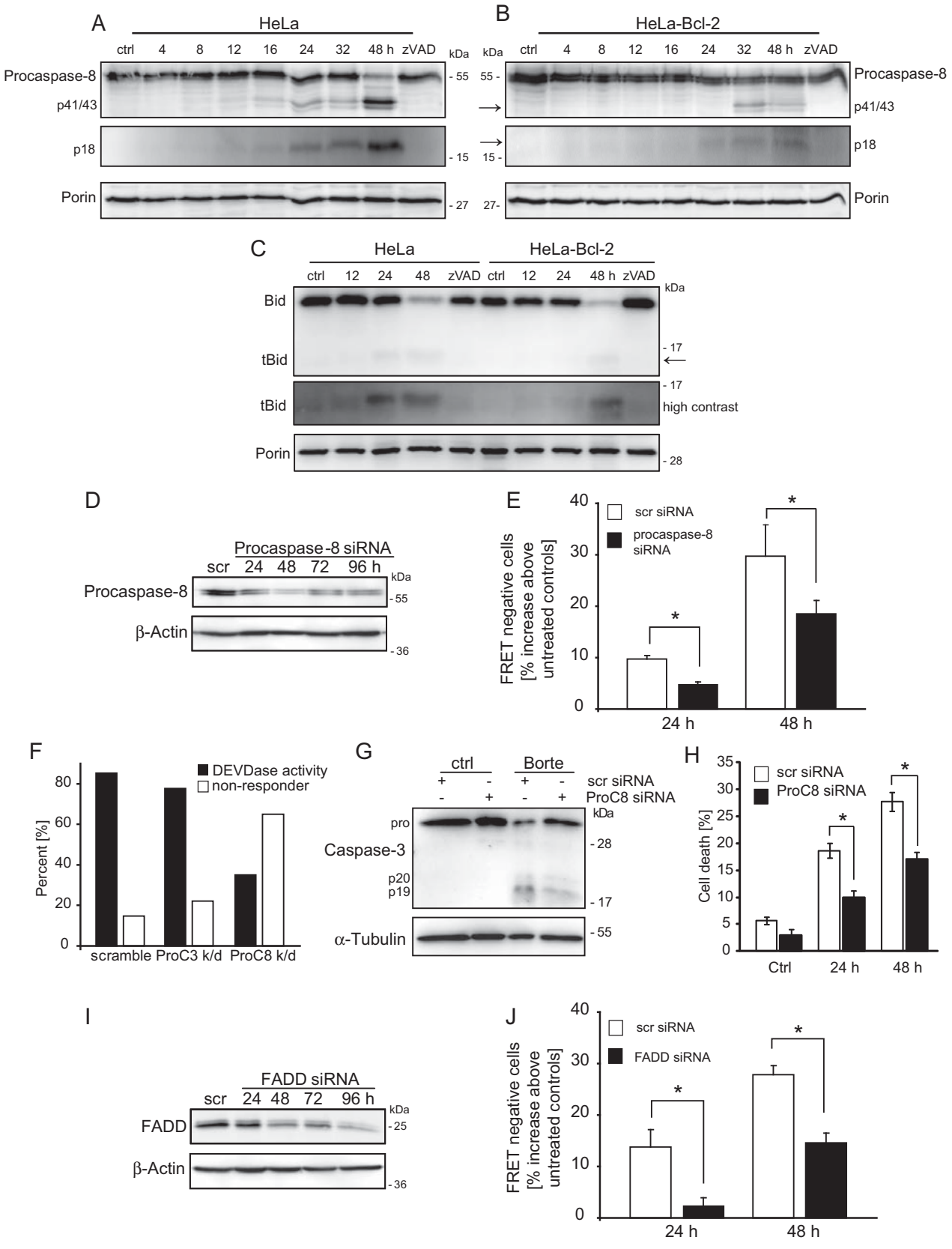
A
HeLa
ctrl 4 8 12 16 24 32 48 h zVAD
kDa
Procaspase-8
p41/43
p18
Porin
- 55
- 15
- 27
B
HeLa-Bcl-2
ctrl 4 8 12 16 24 32 48 h zVAD
kDa
55 -
15 -
27-
Procaspase-8
p41/43
p18
Porin
C
HeLa
HeLa-Bcl-2
ctrl 12 24 48 zVAD ctrl 12 24 48 h zVAD
kDa
Bid
tBid
tBid
high contrast
Porin
- 17
- 17
- 28
D
Procaspase-8 siRNA
scr 24 48 72 96 h
kDa
Procaspase-8
β-Actin
- 55
- 36
E
scr siRNA
procaspase-8 siRNA
FRET negative cells [% increase above untreated controls]
24 h
48 h
F
DEVDase activity
non-responder
Percent [%]
scramble ProC3 k/d ProC8 k/d
G
ctrl
Borte
scr siRNA
ProC8 siRNA
kDa
pro
Caspase-3
p20
p19
α-Tubulin
- 28
- 17
- 55
H
scr siRNA
ProC8 siRNA
Cell death [%]
Ctrl
24 h
48 h
I
FADD siRNA
scr 24 48 72 96 h
kDa
FADD
β-Actin
- 25
- 36
J
scr siRNA
FADD siRNA
FRET negative cells [% increase above untreated controls]
24 h
48 h

Fig. 6

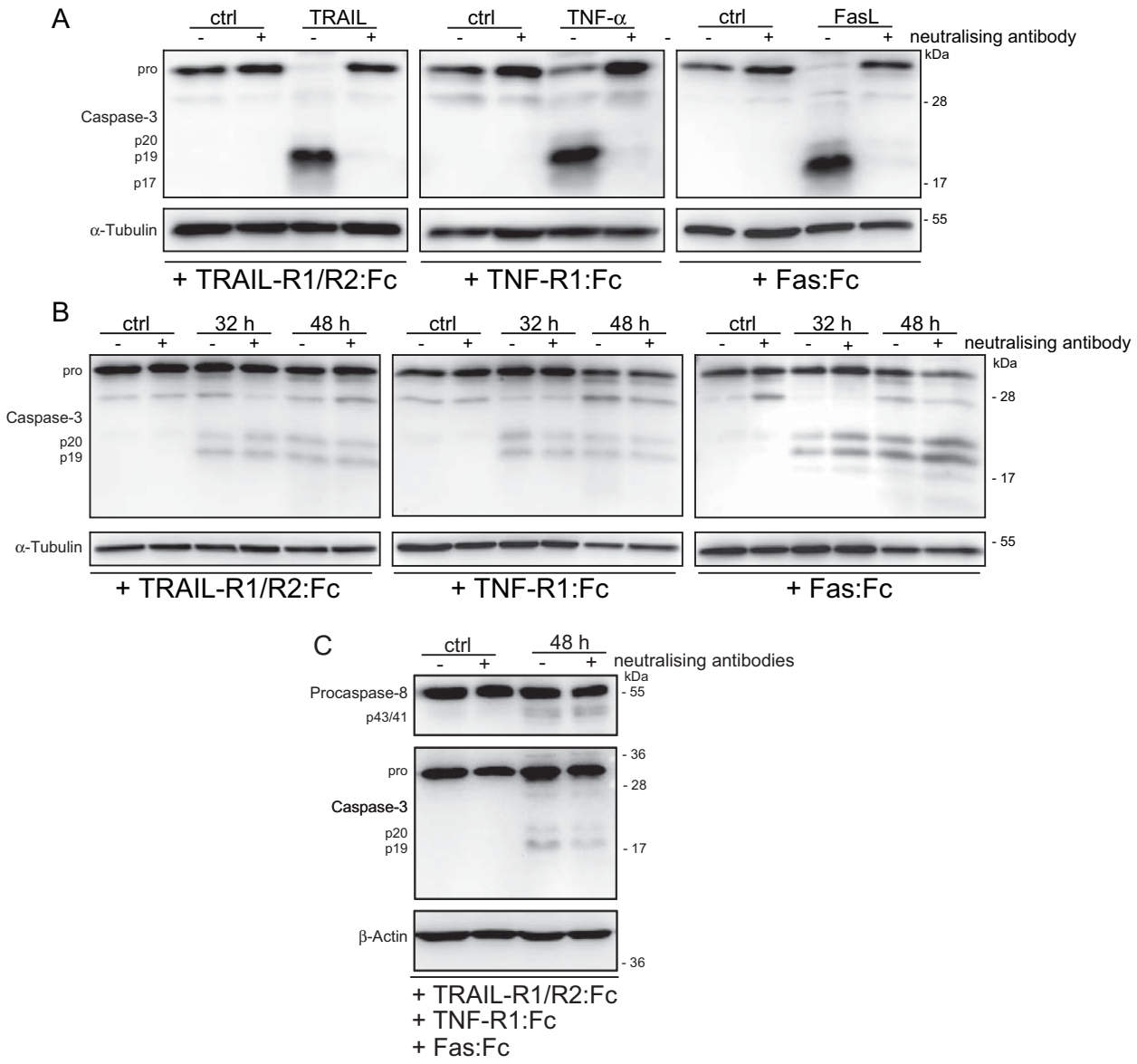
A
ctrl
TRAIL
TNF-α
FasL
neutralising antibody
kDa
pro
Caspase-3
p20
p19
p17
α-Tubulin
- 28
- 17
- 55
+ TRAIL-R1/R2:Fc
+ TNF-R1:Fc
+ Fas:Fc
B
ctrl
32 h
48 h
neutralising antibody
kDa
pro
Caspase-3
p20
p19
α-Tubulin
- 28
- 17
- 55
+ TRAIL-R1/R2:Fc
+ TNF-R1:Fc
+ Fas:Fc
C
ctrl
48 h
neutralising antibodies
kDa
Procaspase-8
p43/41
pro
Caspase-3
p20
p19
β-Actin
- 55
- 36
- 28
- 17
- 36
+ TRAIL-R1/R2:Fc
+ TNF-R1:Fc
+ Fas:Fc

Fig.7

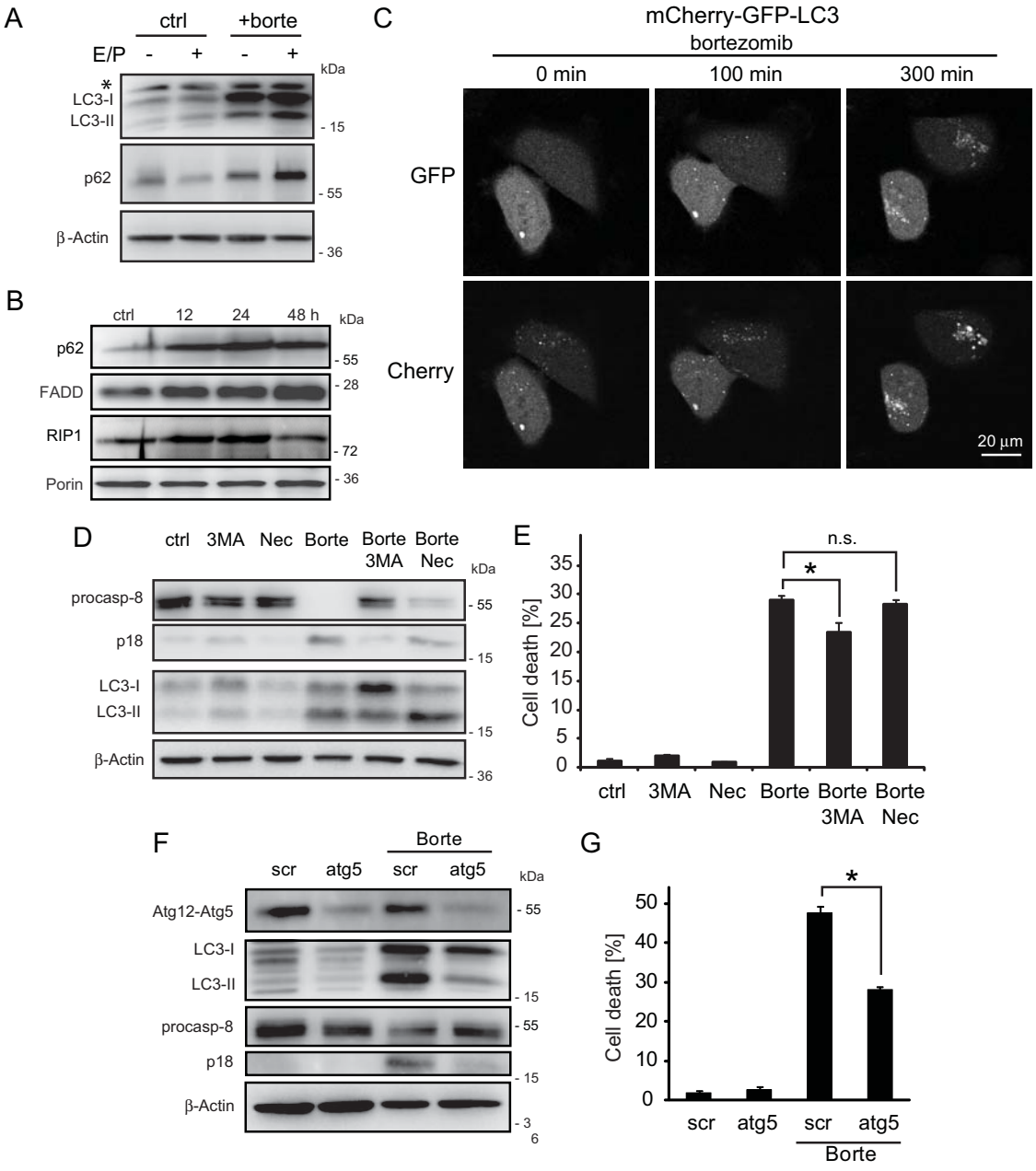
A
ctrl
+borte
E/P - + - +
kDa
*
LC3-I
LC3-II
- 15
p62
- 55
β-Actin
- 36
B
ctrl 12 24 48 h
kDa
p62
- 55
FADD
- 28
RIP1
- 72
Porin
- 36
C
mCherry-GFP-LC3
bortezomib
0 min
100 min
300 min
GFP
Cherry
20 μm
D
ctrl 3MA Nec Borte Borte 3MA Borte Nec
kDa
procasp-8
- 55
p18
- 15
LC3-I
LC3-II
- 15
β-Actin
- 36
E
n.s.
*
Cell death [%]
35
30
25
20
15
10
5
0
ctrl 3MA Nec Borte Borte 3MA Borte Nec
F
Borte
scr atg5 scr atg5
kDa
Atg12-Atg5
- 55
LC3-I
LC3-II
- 15
procasp-8
- 55
p18
- 15
β-Actin
- 3
6
G
*
Cell death [%]
50
40
30
20
10
0
scr atg5 scr atg5
Borte

Fig.8

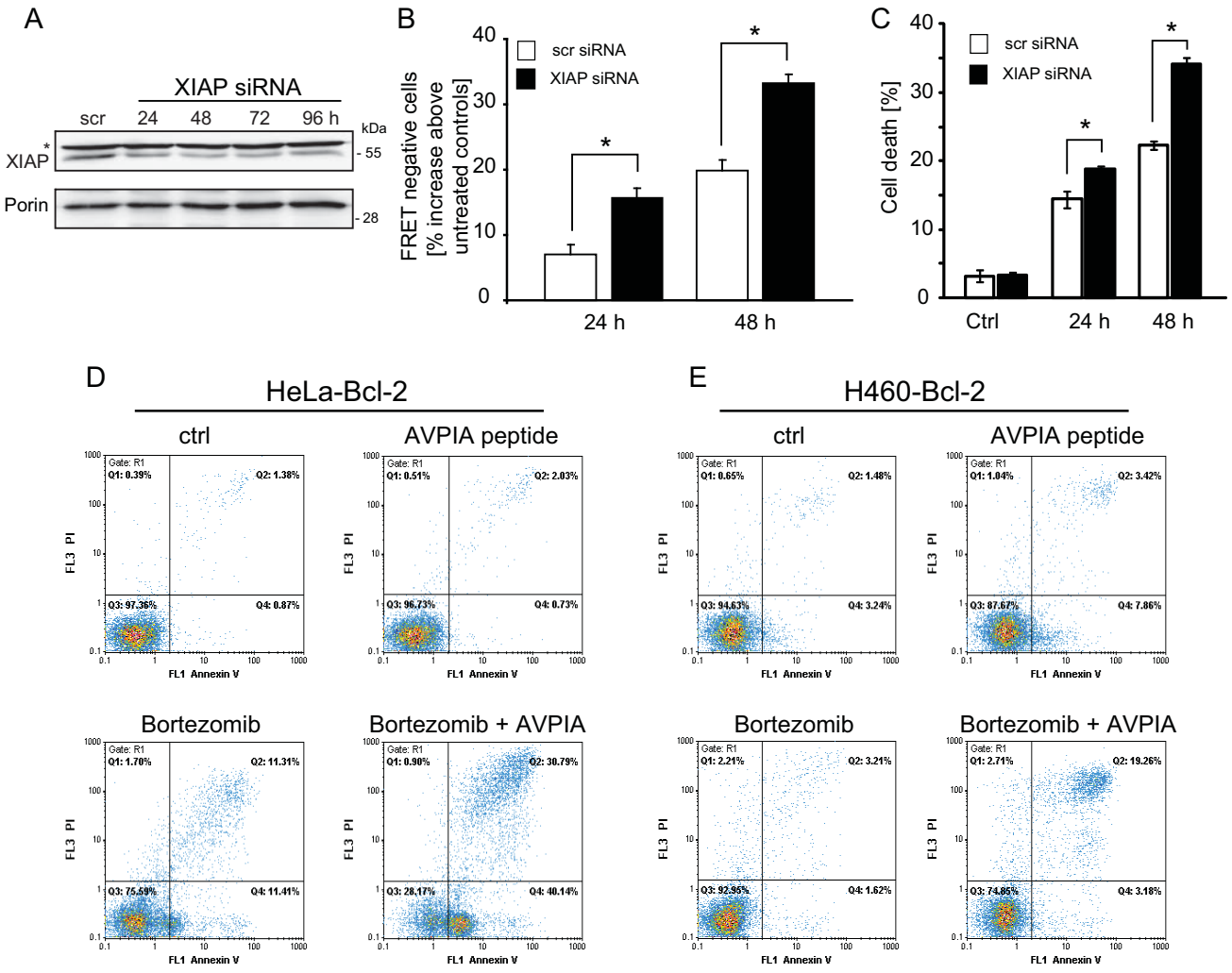
A
XIAP siRNA
scr
24
48
72
96 h
kDa
XIAP
55
Porin
28
B
scr siRNA
XIAP siRNA
FRET negative cells [% increase above untreated controls]
24 h
48 h
C
scr siRNA
XIAP siRNA
Cell death [%]
Ctrl
24 h
48 h
D
HeLa-Bcl-2
ctrl
AVPIA peptide
Bortezomib
Bortezomib + AVPIA
E
H460-Bcl-2
ctrl
AVPIA peptide
Bortezomib
Bortezomib + AVPIA
FL3 PI
FL1 Annexin V